



Published in final edited form as:

*J Neurosci.* 2012 November 14; 32(46): 16314–16330. doi:10.1523/JNEUROSCI.2097-12.2012.

## Post-hearing Ca<sup>2+</sup> Currents and Their Roles in Shaping the Different Modes of Firing of Spiral Ganglion Neurons

Ping Lv<sup>1,2</sup>, Choong-Ryoul Sihm<sup>2</sup>, Wenying Wang<sup>2</sup>, Haitao Shen<sup>1</sup>, Hyo Jeong Kim<sup>2</sup>, Sonia M. Rocha-Sanchez<sup>3</sup>, and Ebenezer N. Yamoah<sup>2,\*</sup>

<sup>1</sup>The Key Laboratory of Neural and Vascular Biology, Ministry of Education, Hebei Medical University, Shijiazhuang, China 050017

<sup>2</sup>University of California, Davis, School of Medicine, Center for Neuroscience, Program in Communication Science, 1544 Newton Ct. Davis CA 95618

<sup>3</sup>Creighton University School of Dentistry, 2500 California Plz, Omaha, NE 68178

### Abstract

Whereas pre-hearing spiral ganglion neurons (SGNs) rely faithfully on outputs from spontaneously active developing hair cells, the electrical phenotypes of post-hearing neurons are shaped by distinct rapid and graded receptor potentials from hair cells. To date, technical difficulties in isolation of fragile post-hearing neurons from the rigid bony labyrinth of the inner ear have hindered analyses of the electrical phenotype of SGNs. Therefore, we have recently developed new strategies to isolate post-hearing mouse SGNs for functional analyses. Here, we describe the coarse and fine properties of Ca<sup>2+</sup> currents, which sculpt the firing properties of post-hearing SGNs. Murine SGNs express multiple Ca<sup>2+</sup> channel currents to confer diverse functions. We have demonstrated that suppression of Ca<sup>2+</sup> currents results in significant hyperpolarization of the resting membrane potential (rmp) of basal SGNs, suggesting that Ca<sup>2+</sup> influx primes rmp for excitation. In contrast, removal of external Ca<sup>2+</sup> has modest effects on rmp of apical SGNs. The blockade of Ca<sup>2+</sup> currents with a cocktail of specific blockers attenuates spontaneously active SGNs. Paradoxically, different subtypes of Ca<sup>2+</sup> currents, such as R-type currents, may activate resting outward conductances since blockage of the current results in depolarization of rmp. In keeping with whole-cell current data, single channel records revealed multiple diverse Ca<sup>2+</sup> channels in SGNs. Additionally, there were differential expressions of distinct Ca<sup>2+</sup> current-densities in the apico-basal contour of the adult cochlea. This report provides invaluable insights into Ca<sup>2+</sup>-dependent processes in adult SGNs.

### Keywords

Hearing; Development; Ca<sup>2+</sup> channels; Voltage-dependent Ca<sup>2+</sup> currents; and Spiral ganglion neurons

### Introduction

The spiral ganglion is the hub from which a set of (type 1) afferent neurons, which constitute ~95% of the total sensory cells (Morrison et al., 1975; Spoendlin, 1981), transmit precise and reliable information about the amplitude, duration and frequency of acoustic waves from hair cells to the cochlear nucleus (CN). Besides the primary role of faithfully encoding

\*Corresponding author with complete address, including an email address: Ebenezer N. Yamoah, Program in Communication Science, Department of Anesthesiology and Pain Medicine, Center for Neuroscience, 1544 Newton Ct., Davis, CA 95618, enyamoah@ucdavis.edu.

acoustic waves from hair cells to the CN, voltage-dependent changes in membrane excitability and corresponding intracellular  $\text{Ca}^{2+}$  ( $\text{Ca}_i^{2+}$ ) fluctuations confer growth and survival of SGNs as well as other  $\text{Ca}^{2+}$ -dependent functions (Hegarty et al., 1997; Roehm et al., 2008). Moreover, a pragmatic role for SGN stimulation and  $\text{Ca}^{2+}$  dependent neuronal survival is reflected in CN cell death following a blockade of SGN activity or cochlear ablation (Pasic and Rubel, 1989), which is underpinned by the utility of cochlear implants in hearing restoration (Leake et al., 1999).

Previous studies have demonstrated the presence of voltage-dependent  $\text{Ca}^{2+}$  currents in SGNs from guinea pigs to embryonic chickens and pre-hearing mice (Yamaguchi and Ohmori, 1990; Hisashi et al., 1995; Jimenez et al., 1997; Chen et al., 2011). Although these studies have provided a wealth of information concerning the histological expression of  $\text{Ca}^{2+}$  channels in pre-hearing neurons, and in one case the properties of L-type  $\text{Ca}^{2+}$  current in guinea pig neurons (Hisashi et al., 1995), little is known about the properties of  $\text{Ca}^{2+}$  currents in post-hearing SGNs, let alone their functions. Meanwhile, immunolocalization of  $\text{Ca}_v1.3$ , 2.1 and 2.3 subunits has been demonstrated in the chinchilla cochlea (Lopez et al., 2003). However, in previous reports in which inner ear tissue was subjected to prolonged fixation and harsh decalcification processes, may have compromised the antigenicity of the channel proteins (Lopez et al., 2003). A set-back in understanding  $\text{Ca}^{2+}$  current functions and membrane properties of SGNs is the lack of recordings from post-hearing adult neurons. Invariably, the prevailing physiological data on ionic currents in SGNs have been obtained from pre-hearing SGNs (Jimenez et al., 1997; Adamson et al., 2002b; Chen et al., 2011) because of technical constraints in isolating and/or recording from fragile neurons in the post-hearing matured bony labyrinth of the inner ear (Adamson et al., 2002a; Jagger and Housley, 2002, 2003).

In this report we have demonstrated that adult murine SGNs rely on the contribution of  $\text{Ca}^{2+}$  influx through  $\text{Ca}^{2+}$  channels to control not only the resting membrane potentials, but also the profile and coding of action potentials. These effects are mediated by multiple  $\text{Ca}^{2+}$  channel currents.  $\text{Ca}^{2+}$  currents fitting into the classification of L-, N, P/Q, R and T-type currents were identified at the whole-cell and single-channel current levels. The corresponding subunits responsible for the assembly of functional channels were localized in the membrane. Finally, differences in current-densities in the apico-basal axis of the adult cochlea may contribute towards the distinct electrical features of apical and basal SGNs. The data presented in this report sets the framework for detailed cellular mechanisms of  $\text{Ca}^{2+}$ -dependent signaling in post-hearing SGNs.

## Materials and Methods

### Isolation of adult spiral ganglion neurons

The present investigation was performed in accordance with the guidelines of the Animal Care and Use Committee of the University of California, Davis. Spiral ganglion neurons (SGNs) were isolated from the mouse inner ear using a combination of enzymatic and mechanical procedures (Wei et al., 2007). Adult male and female (3–4 months old) C57 mice were killed and the temporal bones were removed in a solution containing Minimum Essential Medium with Hank's salt (Invitrogen), 0.2 g/L kynurenic acid, 10 mM  $\text{MgCl}_2$ , 2% fetal bovine serum (FBS; v/v), and glucose (6g/L). The central spiral ganglion tissue was dissected out and split into three equal segments: apical, middle and basal, across the modiolar axis as described (Lv et al., 2010). Previous studies have used apical and basal segments of pre-hearing cochlea to identify extreme differences in membrane properties and ionic current expression in SGNs along the axis of the cochlea (Adamson et al., 2002b; Chen et al., 2011). Since the bony adult preparation was more susceptible to neuronal damage than the cartilaginous pre-hearing cochlea, we used the apical and basal thirds to ensure adequate

viable neuronal yield for the experiments (Lv et al., 2010). Additionally, we pooled three 3–4 month old mice into each SGN culture. A potential drawback in the present study is the paucity of sufficient neurons obtained when the cochlea was divided into more than three segments, as described for pre-hearing cochlea (Chen et al., 2011). Using the basal and apical thirds may produce heterogeneity of SGNs that may potentially mask any apparent distinctions between apical and basal neurons.

The apical and basal tissues were digested separately in an enzyme mixture containing collagenase type I (1 mg/ml), DNase (1 mg/ml) at 37 °C for 20 mins. After a series of gentle triturations and centrifugation in 0.45 M sucrose, the cell pellets were reconstituted in 900 ml culture media (Neuralbasal-A™, supplemented with 2% B27 (v/v), L-glutamine 0.5 mM, penicillin 100 U/ml; Invitrogen), and filtered through a 40- $\mu$ m cell strainer for cell culture and electrophysiological experiments. For adequate voltage-clamp and satisfactory electrophysiological experiments, we cultured SGNs for ~24–48 hrs to allow the detachment of Schwann cells from neuronal membrane surfaces. Additionally, by recording from neurons after ~24–48 hrs after dissociation, we avoided neurons with extensive neurite outgrowth to reduce space clamp problems. An advantage in recording from adult neurons is that neurite outgrowth was less pronounced compared to pre-hearing neurons. Nonetheless, to minimize space clamp artifacts, we targeted spherical neurons with reduced neurite outgrowth for voltage-clamp experiments (Bar-Yehuda and Korngreen, 2008). All electrophysiological experiments were performed at room temperature (21–22°C). Reagents were obtained from Sigma Chemicals (St Louis, MO) unless otherwise specified.

## Electrophysiology

Action potentials were amplified (100X), filtered (bandpass 2–10 kHz), and digitized at 5–500 kHz. Extracellular solution for most experiments contained (in mM) NaCl 145, KCl 6, MgCl<sub>2</sub> 1, CaCl<sub>2</sub> 0–2, D-glucose 10, Hepes 10, at pH 7.3. Alterations of Ca<sup>2+</sup> were adjusted with Mg<sup>2+</sup>. The Ca<sup>2+</sup> concentrations in nominal solutions were measured with a Ca<sup>2+</sup>-sensitive electrode as described (Yamoah et al., 1998). To suppress Ca<sup>2+</sup> influx through Ca<sup>2+</sup> channels, we reduced the external Ca<sup>2+</sup> concentration further to ~10 nM, using custom written software ([maxchelator.stanford.edu/CaMgATPEGTANIST.htm](http://maxchelator.stanford.edu/CaMgATPEGTANIST.htm)). For perforated patch experiments, the tips of the pipettes were filled with the internal solution containing (in mM): KCl 150, Hepes 10, D-glucose 10, at pH 7.3. The pipettes were front-filled with the internal solution and back-filled with the same solution containing 250- $\mu$ g/ml amphotericin.

Whole-cell and cell-attached single channel voltage-clamp recordings of Ca<sup>2+</sup>/Ba<sup>2+</sup> currents were performed on adult SGNs, using an Axopatch 200B amplifier (Molecular Devices, Sunnyvale, CA). Current traces were amplified, filtered (bandpass 2 kHz), and digitized at 5–500 kHz using an analog-to-digital converter, Digidata 1200 (Molecular Devices), as described earlier (Rodriguez-Contreras and Yamoah, 2001; Levic et al., 2007). Fire-polished electrodes (2–3 M $\Omega$ ) were pulled from borosilicate glass. The electrodes contained (in mM): CsCl 70, NMGCl 70, MgCl<sub>2</sub> 1, HEPES 10, EGTA 2–5, CaCl<sub>2</sub> 1, Cs<sub>2</sub>ATP 4, at pH 7.2 with CsOH. The bath solution was constantly perfused (2–3 ml/min) and contained (in mM): CholineCl 120, TEACl 20, 4-AP 5, linopirdine 0.02, CsCl 2, CaCl<sub>2</sub> 1.8–5, MgCl<sub>2</sub> 0.5–5, HEPES 10, D-Glucose 5, at pH 7.40 with NaOH. In all cases when the Ca<sup>2+</sup> concentration was altered, Mg<sup>2+</sup> substitution was used to minimize membrane surface charge effects. Inward Ca<sup>2+</sup> current traces were generated with depolarizing voltage steps from a holding potential of –90/–70 mV and stepped to varying positive potentials ( $\Delta V = 2.5–10$  mV). The capacitive transients were used to estimate the capacitance of the cell as an indirect measure of cell size. The seal resistance was typically 10–15 G $\Omega$ . Currents were measured with capacitance compensation and series resistance compensation (>90%), filtered at 2 kHz using an 8-pole Bessel filter, and sampled at 5 kHz. Given that the maximum current

recorded was  $< 1$  nA, the expected voltage error was  $< 1.5$  mV. The series resistance was monitored during the course of the experiments. The liquid junction potentials were measured and corrected. Besides these standard requirements for acceptance of data, several basic criteria were set to ensure optimum quality of recordings and acceptance of data; these include: 1) Initial stable seals for at least 5 minutes before recordings; 2) Elimination of cells with current traces that exhibit signs of voltage inhomogeneities; 3) Removal of cells with outward current contaminations; and 4) Exclusion of cells with more than 20% change in the series resistance before and during recordings.

Whole-cell  $\text{Ca}^{2+}$  current amplitudes at varying test potentials were measured at the peak and steady-state levels using a peak and steady-state detection routine; the current magnitude was divided by the cell capacitance (pF) to generate the current density-voltage relationship. The stock solutions of all channel blockers and agonists were made either in ddH<sub>2</sub>O or DMSO and stored at  $-20^{\circ}\text{C}$ . The final concentration of DMSO in the recording bath solution was  $\sim 0.0001\%$ . This concentration of DMSO had no effects on action potentials, nor did it alter  $\text{Ca}^{2+}$  current recordings (not shown). The cell-attached configurations of the patch-clamp technique (Hamill et al., 1981) was used to record single  $\text{Ca}^{2+}$  channel currents from adult SGNs. Patch electrodes were pulled from borosilicate glass capillaries with a Flaming-Brown microelectrode puller (P97 Sutter Instr. Co., Navato, CA), coated with Sylgard 184 (Dow-Corning Corp., Midland, MI) to within  $100\ \mu\text{m}$  from the tip, and fire-polished before use. Single-channel recordings of membrane patches were held at  $-90$  or  $-70$  mV, and stepped to different depolarizing test pulses at frequencies between  $0.2$ – $0.5$  Hz. Current traces were amplified and filtered using an 8-pole Bessel filter at  $2$  kHz, and digitized at  $10$  kHz using custom written software. Patch electrodes were filled with a  $\text{Ba}^{2+}$  solution ( $50$  mM) containing (mM)  $20$  N-methyl-D-glucamine (NMG),  $20$  TEACl,  $5$  4-AP, and  $5$  HEPES at pH  $7.4$  (adjusted with TEAOH). The osmolarity of the patch-electrode solution was  $\sim 290$  mosmol. Stock solutions of Bay K 8644 ( $10$  mM) were made in DMSO, and a final concentration of  $5\ \mu\text{M}$  was used. The bath solution contained (mM)  $80$  KCl,  $3$  D-glucose,  $20$  TEACl,  $0.5$   $\text{CaCl}_2$ ,  $5$  4-AP, and  $5$  HEPES at pH  $7.4$  with TEAOH to shift the resting potential to  $\sim 0$  mV (Rodriguez-Contreras & Yamoah, 2003). The  $\text{Ca}^{2+}$  channel blockers, nimodipine (L-type),  $\omega$ -conotoxin MVIIA (CTX; N-type),  $\omega$ -agatoxin IVA (ATX; P/Qtype),  $\omega$ -theraphotoxin-Hg1a,  $\omega$ -TRTX-Hg1a (rSNX-482; R-type) (Alomone Labs, Israel) and mibefradil (T-type) channels were bath-applied for whole-cell and single-channel recordings. Additionally, for single-channel recordings, toxins were backfilled in the pipette solutions for cell-attached experiments. In all cases, liquid junction potentials were measured and corrected as described previously (Rodriguez-Contreras et al., 2002).

For single channel recordings, leakage and capacitive transient currents were subtracted by fitting a smooth template to null traces. Leak-subtracted current recordings were idealized using a half-height criterion (Rodriguez-Contreras and Yamoah, 2001; Rodriguez-Contreras et al., 2008). Transitions between closed and open levels were determined by using a threshold detection algorithm, which required that two data points exist above the half-mean amplitude of the single-unit opening. The computer-detected openings were confirmed by visual inspection, and sweeps with excessive noise were discarded. Amplitude histograms at a given test potential were generated and then fitted to a single Gaussian distribution using a Levenberg-Marquardt algorithm to obtain the mean and standard deviation. At least four voltage steps and their corresponding single-channel currents were used to determine the unitary conductance. Single-channel current-voltage relations were fitted by linear least-square regression lines and single-channel conductances obtained from the slope of the regression lines. Idealized records were used to construct ensemble-averaged currents, open probability, and histograms for the distributions of open and closed intervals. Curve fits and data analyses were performed using Origin software (MicroCal Inc., Northampton, MA). Where appropriate, we presented data in the form of means  $\pm$  S.D (standard deviation). The

mean values (n) listed represent data for each experimental group. Significant differences between groups were tested using paired/unpaired Student's *t* test.

## Immunocytochemistry

Spiral ganglion neurons were isolated from the mouse inner ear and cultured for 48 hrs as described (Lv et al., 2010). Neurons were fixed for 30 mins with 2% paraformaldehyde, washed and then permeabilized in 0.5% Triton X-100 for 5 mins. The samples were incubated for 1 hr in a blocking solution containing phosphate buffered saline (PBS) and 1% horse serum, followed by 3–5 hrs incubation with Ca<sup>2+</sup> channel antibodies against Ca<sub>v</sub>1.3, residues 859–875; Ca<sub>v</sub>2.1, residues 865–881; Ca<sub>v</sub>2.2, residues 851–867 (Alomone, Israel); and Ca<sub>v</sub>2.3, residues 2200-C terminal (Abcam, Cambridge, MA), at 1:100 to 1:500 dilutions. To identify neurons, samples were counter-stained with antibody against the neuronal marker TUJ1 as described (Wei et al., 2008). Cells were then incubated with appropriate secondary antibodies for 2 hrs, washed and mounted using antifade mounting medium, and viewed with a Zeiss LSM 510 confocal microscope.

For histological cryosection experiments, sedated (Avertin (2,2,2,tribromoethanol); 300 µg/gm body weight, i.p.) mice were transcardially perfused with 10 ml PBS followed by 10 ml of 4% paraformaldehyde in 0.1 M PBS. The temporal bones were removed, and the cochleae were perfused *via* the oval and round windows. The temporal bones were then immersed in fixative for 60 mins. After fixation, the cochleae were decalcified (120 mM EDTA, pH 7.0; 24 hrs; ~21°C). Cochleae were processed sequentially with 10% and 30% sucrose at 4 °C overnight then embedded in OTC for cryosection. Sections were washed in PBS, permeabilized in 0.1% Triton X-100 for 25 mins, and then incubated for 30 mins in a blocking solution containing 1% bovine serum albumin and 1% goat serum. The 10-µm sections were incubated with primary antibody overnight at 4°C. The rinsed sections were then incubated (2 hrs; 4°C) in fluorescent dye-conjugated secondary antibody. Images were captured with a Zeiss confocal microscope LSM 510.

## Results

### Effects of Ca<sup>2+</sup> on the membrane properties of adult spiral ganglion neurons

Previous studies have shown that in pre-hearing spiral ganglion, basal neurons are almost all rapidly adapting and apical neurons are a mixture (Adamson et al., 2002a; Adamson et al., 2002b). In post-hearing adult spiral ganglia, neural responses were invariably heterogeneous, ranging from spontaneously active to evoked rapidly adapting neurons in both basal and apical aspects of the cochlea. Thus, we classified neurons not only by their location in the cochlea but also by their evoked firing frequency as rapidly adapting (< 5 Hz), moderately adapting (6–20 Hz), and slowly adapting (> 20 Hz) neurons using 0.2 nA current injection. To determine the coarse features of Ca<sup>2+</sup> currents on membrane properties of SGNs, classical ion substitution experiments were performed by examining evoked action potentials in rapidly (from apical third) and slowly (from basal third) adapting neurons in the presence of bath solutions containing Ca<sup>2+</sup> (2 mM) and nominal Ca<sup>2+</sup> (~100 µM). To minimize changes in membrane potential as a result of surface charge effects, Ca<sup>2+</sup> was replaced with equal concentrations of Mg<sup>2+</sup>. Reduction of Ca<sup>2+</sup> concentration had three noticeable effects on the membrane properties of SGNs. First, the reduction of external Ca<sup>2+</sup> mediated a small but marked membrane hyperpolarization that appeared to be more pronounced in slowly adapting neurons than in rapidly adapting neurons (Fig. 1A–B). Second, as expected from the contribution of Ca<sup>2+</sup> currents towards the upstroke phase of action potentials, the 0 mV overshoot was increased in the presence of external Ca<sup>2+</sup>. In the presence of 2 mM Ca<sup>2+</sup>, the repolarization phase of the action potentials in slowly adapting neurons was more prominent than with nominal Ca<sup>2+</sup> (see legend of figure 1 for summary



data). The effects of increased external  $\text{Ca}^{2+}$  may ensue from the  $\text{Ca}^{2+}$  dependence of activation of  $\text{K}^+$  and/or  $\text{Cl}^-$  currents in SGNs (Adamson et al., 2002b). To further suppress inward  $\text{Ca}^{2+}$  currents, an external solution with a calculated  $\text{Ca}_i^{2+}$  of  $\sim 10$  nM was used (Fig. 1C–I). As amplified in figure 1C, a switch from control to 10-nM- $\text{Ca}^{2+}$  solution resulted in modest hyperpolarization of the resting membrane potential (rmp) of the rapidly adapting apical SGN (rmp at control =  $-58 \pm 6$  mV and in 10-nM  $\text{Ca}^{2+}$  =  $-61 \pm 4$  mV ( $n = 9$ ;  $p = 0.12$ ). The effects of 10-nM external  $\text{Ca}^{2+}$  on action potential profiles were reversible (Fig. 1). In contrast to rapidly adapting neurons, 10-nM external  $\text{Ca}^{2+}$  solution produced significant hyperpolarization of the rmp (Fig. 1E) of the slowly adapting basal neuron. The rmp in the control solution was  $-55 \pm 5$  mV and in the 10-nM- $\text{Ca}^{2+}$  solution it was  $-64 \pm 3$  mV ( $n = 15$ ;  $p < 0.05$ ). Shown in figures 1F–H are reversible effects of the 10-nM- $\text{Ca}^{2+}$  solution on the firing of two classes of non-rapidly adapting basal neurons, namely, moderately (Fig. 1F–H) and slowly adapting neurons (Fig. 1H). Using 0.2-nA current injection for 5-s, moderately adapting basal SGNs in the control solution yielded a mean firing frequency of  $17 \pm 7$  Hz ( $n = 9$ ), which plummeted to  $3 \pm 2$  Hz ( $n = 9$ ;  $p < 0.05$ ) after application of the 10-nM- $\text{Ca}^{2+}$  solution. Upon washout, the control firing pattern was restored to  $12 \pm 7$  Hz ( $n = 9$ ;  $p = 0.08$ ). Meanwhile, in a slowly adapting basal SGN, removal of  $\text{Ca}^{2+}$  currents with the 10-nM  $\text{Ca}^{2+}$  solution reduced the mean firing frequency by  $\sim 4$ -fold, from  $49 \pm 10$  Hz to  $12 \pm 6$  Hz ( $n = 11$ ;  $p < 0.05$ ). The effects of the 10-nM- $\text{Ca}^{2+}$  solution were reversed after a washout with control solutions, recovering to  $39 \pm 14$  Hz ( $n = 11$ ;  $p = 0.11$ ). Whereas suppression of  $\text{Ca}^{2+}$  currents and the ensuing diverse alterations of membrane potential changes in SGNs may result from a single class of  $\text{Ca}^{2+}$  channel currents, it is equally likely that SGNs employ multiple channels to confer  $\text{Ca}^{2+}$ -dependent functions. Exhaustive cellular mechanisms of  $\text{Ca}^{2+}$ -mediated function can be gauged by understanding the transport features of  $\text{Ca}^{2+}$  channel currents.

### Evidence for multiple $\text{Ca}^{2+}$ currents in adult spiral ganglion neurons

To examine  $\text{Ca}^{2+}$  channel currents in SGNs, we suppressed outward  $\text{K}^+$  currents with external TEA, 4-AP, linopirdine, internal  $\text{Cs}^+$ , and  $\text{NMG}^+$  in a manner similar to previous analyses of  $\text{Ca}^{2+}$  current in hair cells (Rodriguez-Contreras and Yamoah, 2001; Adamson et al., 2002b; Rodriguez-Contreras and Yamoah, 2003). Additionally, we curbed contamination of inward  $\text{Ca}^{2+}$  currents by  $\text{Na}^+$  currents by substituting external  $\text{Na}^+$  with choline. The resulting exemplary current traces recorded from a holding voltage of  $-90$  mV and voltage steps ranging from  $-120$  to  $30$  mV with  $\Delta V$  of  $10$  mV are shown in figure 2A (not all current traces were plotted to ensure clarity). Upon shifting the holding voltage to  $-60$  mV and  $-40$  mV (Fig. 2A), the magnitudes of the  $\text{Ca}^{2+}$  current were visibly reduced, and the profiles of the time course of inactivation were altered as well. The difference-current traces between traces elicited from a holding voltage of  $-90$ ,  $-60$  mV, and  $-40$  mV (Fig. 2A) are in keeping with the possibility that membrane hyperpolarization relieves components or different subtypes of  $\text{Ca}^{2+}$  currents from their inactivated states. To further determine whether the apparent differences in the voltage-dependence of the seemingly different subtypes of  $\text{Ca}^{2+}$  currents can be revealed in the current-voltage relation, we used small voltage steps ( $\Delta V = 2.5$  mV) to activate whole-cell  $\text{Ca}^{2+}$  currents and the corresponding current-density-voltage (I–V) curves are plotted as shown in figure 2B. Using a holding potential of  $-90$  mV, the peak current-density was observed at  $\sim -5$  mV. The “shoulder” at  $-35$  to  $-20$  mV may reflect the peak activation of distinct  $\text{Ca}^{2+}$  currents with low-voltage activation properties. Upon holding SGNs at  $-40$  mV, the “shoulder” current was abolished (Fig. 2B) and the “difference” I–V relations suggested the possibility that SGNs express more than one distinct  $\text{Ca}^{2+}$  current subtype. Moreover, to ensure that we were indeed recording  $\text{Ca}^{2+}$  currents, their sensitivity to  $\text{Cd}^{2+}$ , a non-specific  $\text{Ca}^{2+}$  current blocker, was tested as demonstrated in figure 2C. Although the access resistances of our recording conditions were nominal (see methods), kinks in the I–V relations can be

introduced by voltage errors (Yamoah and Crow, 1994; Bar-Yehuda and Korngreen, 2008), so we reduced the magnitude of the current by decreasing the external  $\text{Ca}^{2+}$  from 5 to 2 mM (3 mM  $\text{Mg}^{2+}$  was substituted for  $\text{Ca}^{2+}$ ) to evaluate the kinetics of the tail currents using short (20-ms) and long (200-ms) pre-pulses. Figures 2D–E show that the tail currents elicited with 20-ms pre-pulses were fitted with multiple time constants ( $\tau$ s: three  $\tau$ s) consistent with currents generated from multiple  $\text{Ca}^{2+}$  channel subtypes. Moreover, upon application of 200-ms duration pre-pulses the number of  $\tau$ s was invariably reduced (~two  $\tau$ s; Fig. 2E), raising the possibility that the duration of the pre-pulse was sufficient to cause at least one sub-population of  $\text{Ca}^{2+}$  channel currents to transition into non-conducting states. Analyses of the steady-state inactivation and the kinetics of recovery from inactivation all converged towards the likelihood that SGNs employ more than one  $\text{Ca}^{2+}$  channel subtype to confer  $\text{Ca}^{2+}$  influx (Fig. 2F–G).

### **$\text{Ca}^{2+}$ currents in apical *versus* basal spiral ganglion neurons**

The membrane conductances in SGNs across the cochlear axis are heterogeneous, yielding at least two distinct neurons, namely rapidly and slowly adapting neurons in pre-hearing ganglia (Adamson et al., 2002b). As demonstrated in Figure 1 and later in Figure 5, the diversity of the firing patterns of adult SGNs abound, ranging from spontaneously active to quiescent and rapidly adapting spike-evoked neurons. An intriguing and testable hypothesis is to predict that differential expression of  $\text{Ca}^{2+}$  currents in SGNs contributes towards diverse membrane properties. We examined  $\text{Ca}^{2+}$  current densities in apical one-third *versus* basal one-third of SGNs in the cochlea. Shown in Figure 3A are comparisons of the current densities between apical and basal neurons. The magnitude of  $\text{Ca}^{2+}$  currents in apical neurons was significantly larger than in basal neurons. Moreover, the coarse features of whole-cell  $\text{Ca}^{2+}$  currents may mask other subtle differences that may occur between apical and basal neurons. Thus, we examined the pharmacology of  $\text{Ca}^{2+}$  currents in apical and basal neurons (Fig. 3B–I).

### **Pharmacology of $\text{Ca}^{2+}$ currents in spiral ganglion neurons supports the existence of multiple currents**

After perfusion with bath solution containing 10  $\mu\text{M}$  nifedipine, there was a significant reduction of whole-cell  $\text{Ca}^{2+}$  currents (not shown). To cross check whether the observed effect on the current was dihydropyridine (DHP)-specific, we examined the effects of Bay K8644, the DHP agonist. Consistent with the actions of DHPs on L-type currents, Bay K8644 induced a leftward shift in the activation voltage of the  $\text{Ca}^{2+}$  current by ~15 mV (data not shown). Neuronal and auditory hair cells express L-type  $\text{Ca}^{2+}$  currents that are activated at relatively more negative voltages than their cardiac counterparts (Lewis and Hudspeth, 1983; Perez-Garcia et al., 1995; Platzner et al., 2000; Marcotti et al., 2003; Michna et al., 2003; Schnee and Ricci, 2003; Levic et al., 2007; Zampini et al., 2010). The shift in I–V relation after application of the DHP agonist suggested that the DHP-sensitive current in SGNs belonged to the neuronal L-type current. Because neuronal  $\text{Ca}_v1.3$  channel currents are less sensitive to the DHP antagonists (Xu and Lipscombe, 2001; Helton et al., 2005), and since nimodipine is a more potent blocker (Bean, 1984; Rodriguez-Contreras and Yamoah, 2001), we switched to nimodipine. Shown in Figures 3B–C are representative current traces (insets) and the summary data of the effects of the DHP antagonist on apical *versus* basal SGNs (Table 1). The pharmacology of the DHP-resistant currents was tested further using other known specific organic  $\text{Ca}^{2+}$  current blockers. Using  $\omega$ -Agatoxin IVA (ATX) for P/Q-,  $\omega$ -Conotoxin MVIIA (CTX) for N-, rSNX-482 for R-, mibefradil for T-type  $\text{Ca}^{2+}$  currents, and a cocktail of blockers, we demonstrated that SGNs expressed these multiple current subtypes in apical and basal neurons (Figs. 3–4). The residual current remaining after application of the combined-blocker solution may consist of transient, T-type  $\text{Ca}^{2+}$  currents. In five cells (three basal and two apical) in which the recording conditions were in

accordance with the criteria for accepting data (see methods), a mibefradil-sensitive transient current ensued when cells were held at a holding potential of  $-100$  mV and stepped to depolarizing voltages (Fig. 4C; red trace; mibefradil-sensitive current). The summary data is presented in the current-voltage relationship, which represents data from three basal SGNs.

### Analyses of the contribution of $\text{Ca}^{2+}$ currents on membrane properties

We examined the effects of  $\text{Ca}^{2+}$  currents on membrane potentials first by producing moderate action potential (AP) broadening using external 4-AP ( $250 \mu\text{M}$ ). Action potential width of apical neurons was  $1.9 \pm 0.3$  ms ( $n = 56$ ) and after application of  $250 \mu\text{M}$  4-AP, the action potential width increased to  $4.2 \pm 0.6$  ms (Fig. 5A–B). Moreover, AP width of basal neurons was  $3.2 \pm 0.4$  ms ( $n = 16$ ) and after application of  $250 \mu\text{M}$  4-AP, the AP width increased to  $4.6 \pm 0.7$  ms. In addition to changes in spike width, 4-AP altered the firing pattern of spontaneously active neurons (Fig. 5C). A cocktail of  $\text{Ca}^{2+}$  current blockers, namely nimodipine for L-,  $\omega$ -Agatoxin IVA (ATX) for P/Q-,  $\omega$ -Conotoxin MVIIA (CTX) for N-, rSNX-482 for R-, and mibefradil for T-type currents, rendered spontaneously active neurons quiescent (Fig. 5C). Second, we assessed the effects of individual  $\text{Ca}^{2+}$  current blockers. Shown in Figure 5D is the effect of 4-AP and  $\omega$ -Agatoxin IVA on the rmp. Suppression of the P/Q-type  $\text{Ca}^{2+}$  current resulted in small but consistent depolarization of the rmp. In neurons in which 4-AP-mediated spontaneous action potentials can be observed, application of  $\omega$ -Agatoxin IVA decreased spike amplitude and attenuated spontaneous AP with time (Fig. 5E). For individual spikes, suppression of P/Q-type current produced an increased AP latency duration and increased spike width, as well as suppression of membrane afterhyperpolarization (AHP) (Fig. 5H, Table 2). The findings on the contribution of P/Q type currents were similar but not identical to the role of R-type currents as illustrated in Figure 5J and summarized in Table 2. The mibefradil-sensitive currents contribute towards the upstroke phase, amplitude and latency of APs (Fig. 5F–G). Because suppression of T- P/Q and R-type currents produces prolongation of AP width and reduces the extent of the AHP, it can be inferred that activation of these  $\text{Ca}^{2+}$  currents may mediate activation of unidentified outward currents. The N-type  $\text{Ca}^{2+}$  current produces a modest effect on the AP profile besides prolongation of the latency (Fig. 5I, Table 2). Whereas the use of 4AP-modified action potentials conveniently allowed us to examine the contribution of distinct  $\text{Ca}^{2+}$  channel subtypes in spike waveforms, it is conceivable, albeit unlikely, that a different outcome would have ensued using different concentrations of 4AP and/or other  $\text{K}^+$  current blockers.

### Unitary current properties of single-channel currents in spiral ganglion neurons

To further demonstrate that SGNs express multiple  $\text{Ca}^{2+}$  channel currents, we used a direct approach by recording from single-channel patches in the cell-attached configuration. Figure 6A shows a family of single-channel  $\text{Ba}^{2+}$  current traces recorded from a patch that was held at a holding potential of  $-70$  mV and stepped to voltages indicated in control (Fig. 6A). The charge carrier was  $50$  mM  $\text{Ba}^{2+}$ . Membrane depolarization resulted in typical brief and long openings and, moreover, these long openings were favored at more depolarized potentials in controls and after application of Bay K8644 (Fig. 6B). The amplitude histogram obtained from a test potential of  $-20$  mV is shown (Fig. 6C). Illustrated in Figure 6D is the summary data of the unitary current amplitudes plotted against the test potentials for the dihydropyridine (DHP)-sensitive  $\text{Ca}^{2+}$  channels. The slope conductance for the linear plot is  $22 \pm 3$  pS ( $n = 11$ ). Figure 7 is a layout of cell-attached patch recordings of a family of consecutive Bay K 8644-modified single channel current traces, recorded using  $50$  mM  $\text{Ba}^{2+}$  as the charge carrier from a holding potential of  $-70$  mV and stepped to the  $-10$  mV (left panel) and  $0$  mV (right panel). At more depolarized potentials the channel had frequent long openings, increasing the open probability ( $P_o$ ) that is readily visible in the diary plot



(Fig. 7C) and in the well-resolved increased magnitude of the ensemble-averaged currents (Fig. 7B). The activation of the L-type channel has steep voltage dependence, and a fit to the Boltzmann function revealed a half-activation voltage ( $V_{1/2}$ ) of  $-9.5 \pm 2.4$  mV ( $n = 7$ ) and a maximum slope factor ( $k$ ) of  $4.3 \pm 1.2$  mV ( $n = 7$ ; Fig. 7D). Next, we examined the kinetics of the Bay K 8644-modified single L-type  $\text{Ca}^{2+}$  channels. To ensure that the recordings were made from single L-type channels, only patches containing single-channel events that were blocked by nimodipine were analyzed. Additionally, kinetic analyses were performed on patches that contained only one channel. The criteria consisted of quantitative determination followed by visual inspection of the data (Horn et al., 1991). The patches contained one channel because there was no stacking of events. Furthermore, direct transition from fast to slow kinetics showed similar current amplitude and vice versa, indicating that the gating modes were derived from a single channel. In accordance with a voltage-dependent channel, the time constant of the first latency was faster at more depolarized voltage than hyperpolarized voltage steps (Fig. 7E). Figures 7F–G show open and closed time distributions of single  $\text{Ba}^{2+}$  channel currents. Using 50 mM  $\text{Ba}^{2+}$  as the charged carrier, the channel gating could be described by at least two open and closed states. However, at some step potentials the fast closed time could not be resolved. As shown, for a Bay K 8644-modified channel, patch depolarization increased the duration of long open states as gleaned from the relative dwell times of each component.

We surmised that by exposing SGNs to specific  $\text{Ca}^{2+}$  channel blocker cocktails it should be feasible to resolve the single-channel fluctuations of other  $\text{Ca}^{2+}$  current subtypes that were identified at the whole-cell current level. To record N-type single-channel  $\text{Ba}^{2+}$  currents, we included a cocktail of  $\text{Ca}^{2+}$  channel blockers consisting of 10  $\mu\text{M}$  nimodipine, 1  $\mu\text{M}$   $\omega$ -agatoxin IVA, 200 nM  $\omega$ -theraphotoxin-Hg1a,  $\omega$ -(rSNX-482), and 5  $\mu\text{M}$  mibefradil in the external and patch-electrode solutions. The patch pipette contained 50 mM  $\text{Ba}^{2+}$ . As shown in Fig. 8A, the resulting consecutive single-channel fluctuation traces at different test potentials displayed inward currents that were invariably sustained at test potentials ranging from  $-10$  to 5 mV, from a holding potential of  $-70$  mV. An example of the amplitude histograms used to generate the unitary current amplitude is shown (Fig. 8C). The estimated single-channel conductance (in pS) from the regression line of the I–V relationship was  $19 \pm 2$  pS ( $n = 7$ ) (Fig. 8D). Similar experiments were performed to record P/Q-type single-channel  $\text{Ba}^{2+}$  currents (Fig. 8B). The unitary P/Q-type currents were recorded in bath and patch-pipette solutions containing 10  $\mu\text{M}$  nimodipine, 1  $\mu\text{M}$  conotoxin MVIIA, 200 nM  $\omega$ -(rSNX-482) and 5  $\mu\text{M}$  mibefradil to suppress other  $\text{Ca}^{2+}$  channel currents. As shown the resulting current had openings that were brief and persistent, and the ensuing single channel conductance generated from the regression line of the I–V relationship was  $8.8 \pm 1.6$  pS ( $n = 6$ ) (Fig. 8D). Finally, single-channel  $\text{Ba}^{2+}$  currents from T- and R-type channels were recorded using external and pipette solutions, which suppressed other  $\text{Ca}^{2+}$  channel subtypes except T- and R-type channels (see Fig. 9 legend). Single-channel  $\text{Ba}^{2+}$  currents flowing through T-type channels were recorded with external and pipette solutions containing 10  $\mu\text{M}$  nimodipine, 1  $\mu\text{M}$  conotoxin MVIIA, 200 nM  $\omega$ -(rSNX-482), and 1  $\mu\text{M}$   $\omega$ -agatoxin IVA. Using 50 mM  $\text{Ba}^{2+}$  as the charge carrier, cell-attached patches held at a holding potential of  $-90$  mV and step potentials displayed inward currents that were invariably transient (Fig. 9A). The family of recordings illustrated is from consecutive traces. In another set of experiments when the external and patch pipette solution contained 10  $\mu\text{M}$  nimodipine, 1  $\mu\text{M}$  conotoxin MVIIA, 5  $\mu\text{M}$  mibefradil and 1  $\mu\text{M}$   $\omega$ -agatoxin IVA, the unitary currents had brief openings but persisted throughout the duration of the step voltages. We inferred that these single-channel events resulted from the activity of R-type channels in adult SGNs. Shown in Fig. 9B are R-type single-channel current traces recorded from a holding potential of  $-70$  mV and to the step potentials noted above each set of five consecutive traces. The estimated single-channel conductances (in pS) from the regression

lines of the I–V relationship (Fig. 9C) were  $9.5 \pm 1.3$  (n = 5) and  $14.9 \pm 2.8$  pS (n = 6), for T- and R-type channels, respectively.

### Localization of Ca<sup>2+</sup> channel protein in spiral ganglion neurons

We proceeded to identify Ca<sup>2+</sup> channel subtypes expressed in SGNs using immunofluorescence microscopic methods. We used antibodies against Ca<sub>v</sub>1.3, Ca<sub>v</sub>2.1, Ca<sub>v</sub>2.2, and Ca<sub>v</sub>2.3, and observed positive labeling in the membrane and cytoplasm of SGNs in both apical and basal neurons (Fig. 10). In control experiments whereby SGNs were pre-incubated with purified peptides supplied by the company (data not shown), positive labeling was absent, indicating that the antibodies recognized the targeted sequence. The specificity of the antibodies was not confirmed, however. Using anti-Ca<sub>v</sub>3.1–3 antibodies, we detected consistent positive labeling of the membrane and cytoplasm of apical and basal SGNs (Fig. 10). The labeling was abolished when antibodies were pre-incubated with purified peptides of the respective Ca<sub>v</sub>3.x channels. The expression of the different Ca<sup>2+</sup> channel subtypes in the plasma membrane and cytoplasm is illustrated in Figure 11. To ensure that the data obtained from isolated neurons *in vitro* reflected well with *in vivo* conditions, we repeated the experiments using cryosections of the cochlea (Fig. 12), confirming the existence of multiple Ca<sup>2+</sup> channels in adult SGNs. Thus, biophysical, pharmacological and biochemical analyses divulged from these studies strongly suggest that adult SGNs employ multiple Ca<sup>2+</sup> channel currents to confer diverse Ca<sup>2+</sup>-dependent functions.

### Discussion

The input and output functions of pre-hearing SGNs are distinct from post-hearing neurons. On one hand, the functional coding of action potentials and the wiring of synaptic connections in pre-hearing neurons are thought to be shaped by spontaneous activity from immature hair cells (Kros et al., 1998; Beutner and Moser, 2001; Marcotti et al., 2003; Levic et al., 2007; Tritsch et al., 2007). Moreover, outputs from SGNs to the CN also determine the wiring pattern and neuronal morphology in the brainstem (Deitch and Rubel, 1989b, a; Pasic and Rubel, 1989). These findings underpin the concept that the activity of pre-hearing hair cells and SGNs may sculpt their niche in the constellation of neuronal networks in the auditory pathway. On the other hand, the activity of post-hearing SGNs should match markedly well with rapid and graded receptor potential from hair cells (Palmer and Russell, 1986). At the pivot of the multiple functions of the post-hearing SGN is the contribution of Ca<sup>2+</sup> in shaping the coding pattern by way of Ca<sup>2+</sup> currents and in the activation of Ca<sup>2+</sup>-dependent ionic currents.

The diversity of Ca<sup>2+</sup> currents in SGNs abounds. The implicit assertion from previous reports suggests that because the physiological requisite for Ca<sup>2+</sup>-dependent functions varies in post-hearing SGNs, Ca<sup>2+</sup> currents and Ca<sup>2+</sup> handling in SGNs may differ from pre-hearing neurons. Whereas the  $\alpha$ -subunit of Ca<sub>v</sub>2.1 was expressed robustly in pre-hearing mouse SGNs, it was undetected in adult chinchilla neurons (Lopez et al., 2003; Chen et al., 2011). To ensure accurate representation of the frequency map of the cochlea, the properties of type 1 SGNs vary depending on their apico-basal location (Rusznak et al., 2008; Rusznak and Szucs, 2009). Differences in the membrane properties of apical *versus* basal SGNs have been ascribed to differential expression of distinct K<sup>+</sup> channels, yielding two distinct cell-types, namely fast and slow adapting neurons (Adamson et al., 2002b; Beisel et al., 2005; Chen and Davis, 2006; Bakondi et al., 2009).

First, in contrast to pre-hearing SGNs where the neurons have been categorized into fast and slow adapting neurons, post-hearing neurons are seemingly heterogenous in their firing patterns. There is a wide range of firing patterns in adult neurons; from spontaneously active

to quiescent, that when invoked, results in fast, moderately and slowly adapting neurons. Indeed SGNs from P0–P5 mice have been demonstrated to have intrinsic spontaneous firing (Lin and Chen, 2000). The firing pattern of adult neurons and their place map along the cochlear contour appears not as distinct as it has been reported in pre-hearing neurons (Adamson et al., 2002b; Chen and Davis, 2006). Data presented in Fig 1A and D suggests that  $\text{Ca}^{2+}$  channels constitute ~50% of the spike amplitude. Moreover, the effects of nominal  $\text{Ca}^{2+}$  (~100  $\mu\text{M}$ ), specifically spike overshoots, were masked in experiments using nanomolar  $\text{Ca}^{2+}$ .  $\text{Mg}^{2+}$  substitution for  $\text{Ca}^{2+}$  might have eliminated surface charge screening effects of divalent cations however, other effects of  $\text{Mg}^{2+}$  on  $\text{Na}^+$  and  $\text{K}^+$  currents are likely to mask the genuine effects of reduction of external  $\text{Ca}^{2+}$  (Negulyaev and Markwardt, 2000; Murata et al., 2002). Additionally, the voltage-dependence of activation and inactivation of  $\text{Na}^+$  currents depend on  $\text{Ca}_i^{2+}$  modulation (Biswas et al., 2009).  $\text{Na}^+$  channels are exquisitely sensitive to available  $\text{Ca}_i^{2+}$ , (Horn, 1999; Wingo et al., 2004). Thus, it is plausible to speculate that by reducing external  $\text{Ca}^{2+}$ ,  $\text{Na}^+$  currents, may be enhanced, producing an aberrant increase in the action potential overshoot.

Second, we have recently employed strategies to isolate adult mice SGNs (Lv et al., 2010), and in this report have described in detail the composition of multiple  $\text{Ca}^{2+}$  currents in post-hearing neurons. The findings are as follows: 1) The magnitude of  $\text{Ca}^{2+}$  current density was markedly larger in post-hearing SGNs at the apical rather than at the basal turn of the cochlea. 2) Evidence for functional expression of multiple  $\text{Ca}^{2+}$  currents in adult SGNs can be gleaned from disparate closing kinetics of the whole-cell  $\text{Ca}^{2+}$  currents (Armstrong and Matteson, 1985, 1986). 3) Voltage-dependent activation/deactivation and inactivation criteria, as well as pharmacological indexes, have further ascertained that adult SGNs harbor  $\text{Ca}_v1.3$  (L-type),  $\text{Ca}_v2.1$  (P/Q-type),  $\text{Ca}_v2.2$  (N-type), and  $\text{Ca}_v2.3$  (R-type) channels (Catterall et al., 2005) (Table 3). These channels constitute ~70% and 80% of the total  $\text{Ca}^{2+}$  currents at basal and apical turns of the cochlea, respectively. The remaining current may be derived from  $\text{Ca}_v3$  (T-type) channels. 4) Data gleaned from pharmacological dissection of post-hearing SGNs dovetailed well with the *in vitro* and *in vivo* immunolabeling analyses. A note of caution on the pharmacological analysis should be highlighted however, as some of the  $\text{Ca}^{2+}$  channel blockers, *e.g.* the dihydropyridines, have been found to block  $\text{K}^+$  currents as well. Thus, the non-specific effects of the  $\text{Ca}^{2+}$  channel blockers cannot be ruled out (Zhang and Gold, 2009). Block of  $\text{Ca}^{2+}$  currents may produce functional alteration of  $\text{Ca}^{2+}$ -activated  $\text{K}^+$  current ( $\text{I}_{\text{KCa}}$ ), which may be manifested as increased neuronal excitability (Gu et al., 2007). Alternatively, enhanced  $\text{I}_{\text{KCa}}$  can produce similar effects by inducing membrane hyperpolarization resulting in removal of  $\text{Na}^+$  channels from inactivation (Du et al., 2005). Moreover the proximity of  $\text{I}_{\text{KCa}}$  channels and the effectiveness of  $\text{Ca}^{2+}_i$  buffers can play important roles on the physiological outcomes. 5) The L- and N- type currents may be disproportionately expressed along the tonotopic axis of the cochlea, such that apical neurons express substantially larger currents than basal neurons. If spike frequency adaptation in SGNs is  $\text{Ca}^{2+}$  dependent *via*  $\text{I}_{\text{KCa}}$ , as has been documented in other systems (Lorenzon and Foehring, 1992; Kim and Rieke, 2001; Groth et al., 2011), it would be consistent with the finding that apical neurons express larger  $\text{Ca}^{2+}$  current magnitude than basal neurons. 6) By measuring the single-channel fluctuations of  $\text{Ca}^{2+}$  channel current subtypes, we have demonstrated that the L-, N-, P/Q-, R- and T- type channels in adult SGNs are distinct with conductance (in pS) of ~22, 19, 9, 15, and 10, respectively. Differences in conductances invariably result from the concentrations and divalent cations used as charge carriers for  $\text{Ca}^{2+}$  channels (Church and Stanley, 1996; Rodriguez-Contreras and Yamoah, 2001; Rodriguez-Contreras et al., 2002; Rodriguez-Contreras et al., 2008). The concentrations of  $\text{Ba}^{2+}$  (50 mM) used as a charge carrier is expected to impose a surface charge effect, producing a rightward shift in the voltage-dependence of activation (Hagiwara and Takahashi, 1967). The  $V_{1/2}$  obtained for the L-type channel ( $-9.5 \pm 2.4$  mV) would be expected to shift by ~18 mV in hyperpolarized direction if the experiments were conducted

in 5 mM Ba<sup>2+</sup>, resulting in values that are comparable to previous reports on the L-type channels in hair cells from the bullfrog saccule (Rodriguez-Contreras and Yamoah, 2003) and mouse cochlear hair cells (Zampini et al., 2010).

Differential and heterogeneous expression of Ca<sup>2+</sup> channels along the frequency map of the cochlea of pre-hearing SGNs have been demonstrated, and, similar to previous studies, the expressions of Ca<sub>v</sub>1.3, Ca<sub>v</sub>2.2 and Ca<sub>v</sub>3.3 have been confirmed to be neuron-specific (Chen et al., 2011). In contrast, post-hearing SGNs have been shown to express additional Ca<sup>2+</sup> channels, namely Ca<sub>v</sub>1.2 and Ca<sub>v</sub>3.1 (Lopez et al., 2003). A recent report has demonstrated that ~90% of the presynaptic Ca<sup>2+</sup> currents of P11 SGNs at the bushy cell synapse is of the P/Q type (Lin et al., 2011). Thus, differential expression of Ca<sup>2+</sup> channel subtypes as seen along the cochlear contour, may also take place along the soma-axonal axis of SGNs. The complex distribution pattern of Ca<sup>2+</sup> channels in SGNs is underpinned by the findings that Schwann cell ensheathments of neurons are also endowed with multiple Ca<sup>2+</sup> channels (Chen et al., 2011), making it difficult, especially when immunolabeling is only used in the *in vivo* setting, to distinguish between neuron *versus* Schwann cell-specific Ca<sup>2+</sup> channel subtypes. In this study, we circumvent the masking effects of glial-cell Ca<sup>2+</sup> currents, since dissociated SGNs lose their glial cell after ~48 hours. Thus, the current study unequivocally demonstrates that SGNs express at least five distinct Ca<sup>2+</sup> channel.

Control of Ca<sub>i</sub><sup>2+</sup> and spatial and temporal separation of Ca<sup>2+</sup> signaling pathways is achieved by several means, including: fixed and diffusible endogenous Ca<sup>2+</sup> buffers, Ca<sup>2+</sup> stores, and Ca<sup>2+</sup> extrusion mechanisms (Meinrenken et al., 2003). An alternative mechanism is to assign different Ca<sup>2+</sup> channel domains to diverse functions through Ca<sup>2+</sup> channel clusters and Ca<sup>2+</sup> channel subtypes (Rodriguez-Contreras and Yamoah, 2001). In contrast to hair cells in which the predominant Ca<sup>2+</sup> current is derived from neuronal Cav1.3 channel current (Platzter et al., 2000; Rodriguez-Contreras and Yamoah, 2001; Dou et al., 2004; Zampini et al., 2010), SGNs employ multiple Ca<sup>2+</sup> currents to confer Ca<sup>2+</sup>-dependent functions. These functions range from sculpting the shape, duration and modulation of K<sup>+</sup> currents to determine the contour of afterhyperpolarization, of action potentials. At the presynaptic sites Ca<sup>2+</sup>-mediated transmitter release can be conferred by a few distinct channels (Borst and Sakmann, 1999; Lin et al., 2011). Moreover, the potential role of Ca<sup>2+</sup> channels (e.g. Ca<sub>v</sub>1.2 channels) in excitation-transcription coupling in SGNs, may require future investigations (Dolmetsch et al., 2001; Marshall et al., 2011). Thus, the next phase of understanding Ca<sup>2+</sup>-mediated signaling in SGNs would be to identify Ca<sup>2+</sup> channel subtype-specific functions.

## Acknowledgments

We thank members of our laboratory for comments on the manuscript. This work was supported by grants to ENY from the NIH (DC003826). PL was funded by the National Organization for Hearing Research.

## References

- Adamson CL, Reid MA, Davis RL. Opposite actions of brain-derived neurotrophic factor and neurotrophin-3 on firing features and ion channel composition of murine spiral ganglion neurons. *The Journal of neuroscience : the official journal of the Society for Neuroscience*. 2002a; 22:1385–1396. [PubMed: 11850465]
- Adamson CL, Reid MA, Mo ZL, Bowne-English J, Davis RL. Firing features and potassium channel content of murine spiral ganglion neurons vary with cochlear location. *The Journal of comparative neurology*. 2002b; 447:331–350. [PubMed: 11992520]
- Armstrong CM, Matteson DR. Two distinct populations of calcium channels in a clonal line of pituitary cells. *Science*. 1985; 227:65–67. [PubMed: 2578071]

- Armstrong CM, Matteson DR. The role of calcium ions in the closing of K channels. *The Journal of general physiology*. 1986; 87:817–832. [PubMed: 2425040]
- Bakondi G, Por A, Kovacs I, Szucs G, Rusznak Z. Hyperpolarization-activated, cyclic nucleotide-gated, cation non-selective channel subunit expression pattern of guinea-pig spiral ganglion cells. *Neuroscience*. 2009; 158:1469–1477. [PubMed: 19038312]
- Bar-Yehuda D, Korngreen A. Space-clamp problems when voltage clamping neurons expressing voltage-gated conductances. *Journal of neurophysiology*. 2008; 99:1127–1136. [PubMed: 18184885]
- Bean BP. Nitrendipine block of cardiac calcium channels: high-affinity binding to the inactivated state. *Proceedings of the National Academy of Sciences of the United States of America*. 1984; 81:6388–6392. [PubMed: 6093100]
- Beisel KW, Rocha-Sanchez SM, Morris KA, Nie L, Feng F, Kachar B, Yamoah EN, Fritzsche B. Differential expression of KCNQ4 in inner hair cells and sensory neurons is the basis of progressive high-frequency hearing loss. *The Journal of neuroscience : the official journal of the Society for Neuroscience*. 2005; 25:9285–9293. [PubMed: 16207888]
- Beutner D, Moser T. The presynaptic function of mouse cochlear inner hair cells during development of hearing. *The Journal of neuroscience : the official journal of the Society for Neuroscience*. 2001; 21:4593–4599. [PubMed: 11425887]
- Biswas S, DiSilvestre D, Tian Y, Halperin VL, Tomaselli GF. Calcium-mediated dual-mode regulation of cardiac sodium channel gating. *Circ Res*. 2009; 104:870–878. [PubMed: 19265034]
- Borst JG, Sakmann B. Effect of changes in action potential shape on calcium currents and transmitter release in a calyx-type synapse of the rat auditory brainstem. *Philos Trans R Soc Lond B Biol Sci*. 1999; 354:347–355. [PubMed: 10212483]
- Catterall WA, Perez-Reyes E, Snutch TP, Striessnig J. International Union of Pharmacology. XLVIII. Nomenclature and structure-function relationships of voltage-gated calcium channels. *Pharmacol Rev*. 2005; 57:411–425. [PubMed: 16382099]
- Chen WC, Davis RL. Voltage-gated and two-pore-domain potassium channels in murine spiral ganglion neurons. *Hear Res*. 2006; 222:89–99. [PubMed: 17079103]
- Chen WC, Xue HZ, Hsu YL, Liu Q, Patel S, Davis RL. Complex distribution patterns of voltage-gated calcium channel alpha-subunits in the spiral ganglion. *Hear Res*. 2011
- Church PJ, Stanley EF. Single L-type calcium channel conductance with physiological levels of calcium in chick ciliary ganglion neurons. *The Journal of physiology*. 1996; 496 ( Pt 1):59–68. [PubMed: 8910196]
- Deitch JS, Rubel EW. Changes in neuronal cell bodies in N. laminaris during deafferentation-induced dendritic atrophy. *The Journal of comparative neurology*. 1989a; 281:259–268. [PubMed: 2708576]
- Deitch JS, Rubel EW. Rapid changes in ultrastructure during deafferentation-induced dendritic atrophy. *The Journal of comparative neurology*. 1989b; 281:234–258. [PubMed: 2708575]
- Dolmetsch RE, Pajvani U, Fife K, Spotts JM, Greenberg ME. Signaling to the nucleus by an L-type calcium channel-calmodulin complex through the MAP kinase pathway. *Science*. 2001; 294:333–339. [PubMed: 11598293]
- Dou H, Vazquez AE, Namkung Y, Chu H, Cardell EL, Nie L, Parson S, Shin HS, Yamoah EN. Null mutation of alpha1D Ca<sup>2+</sup> channel gene results in deafness but no vestibular defect in mice. *J Assoc Res Otolaryngol*. 2004; 5:215–226. [PubMed: 15357422]
- Du W, Bautista JF, Yang H, Diez-Sampedro A, You SA, Wang L, Kotagal P, Luders HO, Shi J, Cui J, Richerson GB, Wang QK. Calcium-sensitive potassium channelopathy in human epilepsy and paroxysmal movement disorder. *Nat Genet*. 2005; 37:733–738. [PubMed: 15937479]
- Groth RD, Lindskog M, Thiagarajan TC, Li L, Tsien RW. Beta Ca<sup>2+</sup>/CaM-dependent kinase type II triggers upregulation of GluA1 to coordinate adaptation to synaptic inactivity in hippocampal neurons. *Proceedings of the National Academy of Sciences of the United States of America*. 2011; 108:828–833. [PubMed: 21187407]
- Gu N, Vervaeke K, Storm JF. BK potassium channels facilitate high-frequency firing and cause early spike frequency adaptation in rat CA1 hippocampal pyramidal cells. *The Journal of physiology*. 2007; 580:859–882. [PubMed: 17303637]



- Hagiwara S, Takahashi K. Surface density of calcium ions and calcium spikes in the barnacle muscle fiber membrane. *The Journal of general physiology*. 1967; 50:583–601. [PubMed: 11526848]
- Hamill OP, Marty A, Neher E, Sakmann B, Sigworth FJ. Improved patch-clamp techniques for high-resolution current recording from cells and cell-free membrane patches. *Pflugers Arch*. 1981; 391:85–100. [PubMed: 6270629]
- Hegarty JL, Kay AR, Green SH. Trophic support of cultured spiral ganglion neurons by depolarization exceeds and is additive with that by neurotrophins or cAMP and requires elevation of  $[Ca^{2+}]_i$  within a set range. *The Journal of neuroscience : the official journal of the Society for Neuroscience*. 1997; 17:1959–1970. [PubMed: 9045725]
- Helton TD, Xu W, Lipscombe D. Neuronal L-type calcium channels open quickly and are inhibited slowly. *The Journal of neuroscience : the official journal of the Society for Neuroscience*. 2005; 25:10247–10251. [PubMed: 16267232]
- Hisashi K, Nakagawa T, Yasuda T, Kimitsuki T, Komune S, Komiyama S. Voltage-dependent  $Ca^{2+}$  channels in the spiral ganglion cells of guinea pig cochlea. *Hear Res*. 1995; 91:196–201. [PubMed: 8647721]
- Horn F, Bilezikjian LM, Perrin MH, Bosma MM, Windle JJ, Huber KS, Blount AL, Hille B, Vale W, Mellon PL. Intracellular Responses to Gonadotropin-Releasing-Hormone in a Clonal Cell-Line of the Gonadotrope Lineage. *Molecular Endocrinology*. 1991; 5:347–355. [PubMed: 1653891]
- Horn R. The dual role of calcium: pore blocker and modulator of gating. *Proceedings of the National Academy of Sciences of the United States of America*. 1999; 96:3331–3332. [PubMed: 10097036]
- Jagger DJ, Housley GD. A-type potassium currents dominate repolarisation of neonatal rat primary auditory neurones in situ. *Neuroscience*. 2002; 109:169–182. [PubMed: 11784708]
- Jagger DJ, Housley GD. Membrane properties of type II spiral ganglion neurones identified in a neonatal rat cochlear slice. *The Journal of physiology*. 2003; 552:525–533. [PubMed: 14561834]
- Jimenez C, Gireldez F, Represa J, Garcia-Diaz JF. Calcium currents in dissociated cochlear neurons from the chick embryo and their modification by neurotrophin-3. *Neuroscience*. 1997; 77:673–682. [PubMed: 9070744]
- Kim KJ, Rieke F. Temporal contrast adaptation in the input and output signals of salamander retinal ganglion cells. *The Journal of neuroscience : the official journal of the Society for Neuroscience*. 2001; 21:287–299. [PubMed: 11150346]
- Kros CJ, Ruppersberg JP, Rusch A. Expression of a potassium current in inner hair cells during development of hearing in mice. *Nature*. 1998; 394:281–284. [PubMed: 9685158]
- Leake PA, Hradek GT, Snyder RL. Chronic electrical stimulation by a cochlear implant promotes survival of spiral ganglion neurons after neonatal deafness. *The Journal of comparative neurology*. 1999; 412:543–562. [PubMed: 10464355]
- Levic S, Nie L, Tuteja D, Harvey M, Sokolowski BH, Yamoah EN. Development and regeneration of hair cells share common functional features. *Proceedings of the National Academy of Sciences of the United States of America*. 2007; 104:19108–19113. [PubMed: 18025474]
- Lewis RS, Hudspeth AJ. Voltage- and ion-dependent conductances in solitary vertebrate hair cells. *Nature*. 1983; 304:538–541. [PubMed: 6603579]
- Lin KH, Oleskevich S, Taschenberger H. Presynaptic  $Ca^{2+}$  influx and vesicle exocytosis at the mouse endbulb of Held: a comparison of two auditory nerve terminals. *The Journal of physiology*. 2011; 589:4301–4320. [PubMed: 21746778]
- Lin X, Chen S. Endogenously generated spontaneous spiking activities recorded from postnatal spiral ganglion neurons in vitro. *Brain research Developmental brain research*. 2000; 119:297–305. [PubMed: 10675781]
- Lopez I, Ishiyama G, Acuna D, Ishiyama A, Baloh RW. Immunolocalization of voltage-gated calcium channel  $\alpha_1$  subunits in the chinchilla cochlea. *Cell Tissue Res*. 2003; 313:177–186. [PubMed: 12845523]
- Lorenzon NM, Foehring RC. Relationship between repetitive firing and afterhyperpolarizations in human neocortical neurons. *Journal of neurophysiology*. 1992; 67:350–363. [PubMed: 1373765]
- Lv P, Wei D, Yamoah EN. Kv7-type channel currents in spiral ganglion neurons: involvement in sensorineural hearing loss. *J Biol Chem*. 2010; 285:34699–34707. [PubMed: 20739290]

- Marcotti W, Johnson SL, Rusch A, Kros CJ. Sodium and calcium currents shape action potentials in immature mouse inner hair cells. *The Journal of physiology*. 2003; 552:743–761. [PubMed: 12937295]
- Marshall MR, Clark JP 3rd, Westenbroek R, Yu FH, Scheuer T, Catterall WA. Functional roles of a C-terminal signaling complex of CaV1 channels and A-kinase anchoring protein 15 in brain neurons. *J Biol Chem*. 2011; 286:12627–12639. [PubMed: 21224388]
- Meinrenken CJ, Borst JG, Sakmann B. Local routes revisited: the space and time dependence of the Ca<sup>2+</sup> signal for phasic transmitter release at the rat calyx of Held. *The Journal of physiology*. 2003; 547:665–689. [PubMed: 12562955]
- Michna M, Knirsch M, Hoda JC, Muenkner S, Langer P, Platzer J, Striessnig J, Engel J. Cav1.3 (alpha1D) Ca<sup>2+</sup> currents in neonatal outer hair cells of mice. *The Journal of physiology*. 2003; 553:747–758. [PubMed: 14514878]
- Morrison D, Schindler RA, Wersall J. A quantitative analysis of the afferent innervation of the organ of corti in guinea pig. *Acta Otolaryngol*. 1975; 79:11–23. [PubMed: 1146528]
- Murata Y, Fujiwara Y, Kubo Y. Identification of a site involved in the block by extracellular Mg(2+) and Ba(2+) as well as permeation of K(+) in the Kir2.1 K(+) channel. *The Journal of physiology*. 2002; 544:665–677. [PubMed: 12411513]
- Negulyaev YA, Markwardt F. Block by extracellular Mg<sup>2+</sup> of single human purinergic P2X4 receptor channels expressed in human embryonic kidney cells. *Neuroscience letters*. 2000; 279:165–168. [PubMed: 10688055]
- Palmer AR, Russell IJ. Phase-locking in the cochlear nerve of the guinea-pig and its relation to the receptor potential of inner hair-cells. *Hear Res*. 1986; 24:1–15. [PubMed: 3759671]
- Pasic TR, Rubel EW. Rapid changes in cochlear nucleus cell size following blockade of auditory nerve electrical activity in gerbils. *The Journal of comparative neurology*. 1989; 283:474–480. [PubMed: 2745750]
- Perez-Garcia MT, Kamp TJ, Marban E. Functional properties of cardiac L-type calcium channels transiently expressed in HEK293 cells. Roles of alpha 1 and beta subunits. *The Journal of general physiology*. 1995; 105:289–305. [PubMed: 7539049]
- Platzer J, Engel J, Schrott-Fischer A, Stephan K, Bova S, Chen H, Zheng H, Striessnig J. Congenital deafness and sinoatrial node dysfunction in mice lacking class D L-type Ca<sup>2+</sup> channels. *Cell*. 2000; 102:89–97. [PubMed: 10929716]
- Rodriguez-Contreras A, Yamoah EN. Direct measurement of single-channel Ca(2+) currents in bullfrog hair cells reveals two distinct channel subtypes. *The Journal of physiology*. 2001; 534:669–689. [PubMed: 11483699]
- Rodriguez-Contreras A, Yamoah EN. Effects of permeant ion concentrations on the gating of L-type Ca<sup>2+</sup> channels in hair cells. *Biophys J*. 2003; 84:3457–3469. [PubMed: 12719271]
- Rodriguez-Contreras A, Nonner W, Yamoah EN. Ca<sup>2+</sup> transport properties and determinants of anomalous mole fraction effects of single voltage-gated Ca<sup>2+</sup> channels in hair cells from bullfrog sacculle. *The Journal of physiology*. 2002; 538:729–745. [PubMed: 11826161]
- Rodriguez-Contreras A, Lv P, Zhu J, Kim HJ, Yamoah EN. Effects of strontium on the permeation and gating phenotype of calcium channels in hair cells. *Journal of neurophysiology*. 2008; 100:2115–2124. [PubMed: 18701758]
- Roehm PC, Xu N, Woodson EA, Green SH, Hansen MR. Membrane depolarization inhibits spiral ganglion neurite growth via activation of multiple types of voltage sensitive calcium channels and calpain. *Mol Cell Neurosci*. 2008; 37:376–387. [PubMed: 18055215]
- Rusznak Z, Szucs G. Spiral ganglion neurones: an overview of morphology, firing behaviour, ionic channels and function. *Pflugers Arch*. 2009; 457:1303–1325. [PubMed: 18777041]
- Rusznak Z, Bakondi G, Pocsai K, Por A, Kosztka L, Pal B, Nagy D, Szucs G. Voltage-gated potassium channel (Kv) subunits expressed in the rat cochlear nucleus. *J Histochem Cytochem*. 2008; 56:443–465. [PubMed: 18256021]
- Schnee ME, Ricci AJ. Biophysical and pharmacological characterization of voltage-gated calcium currents in turtle auditory hair cells. *The Journal of physiology*. 2003; 549:697–717. [PubMed: 12740421]

- Spoendlin H. Differentiation of cochlear afferent neurons. *Acta Otolaryngol.* 1981; 91:451–456. [PubMed: 7023177]
- Tritsch NX, Yi E, Gale JE, Glowatzki E, Bergles DE. The origin of spontaneous activity in the developing auditory system. *Nature.* 2007; 450:50–55. [PubMed: 17972875]
- Wei D, Jin Z, Jarlebark L, Scarfone E, Ulfendahl M. Survival, synaptogenesis, and regeneration of adult mouse spiral ganglion neurons in vitro. *Dev Neurobiol.* 2007; 67:108–122. [PubMed: 17443776]
- Wei D, Levic S, Nie L, Gao WQ, Petit C, Jones EG, Yamoah EN. Cells of adult brain germinal zone have properties akin to hair cells and can be used to replace inner ear sensory cells after damage. *Proceedings of the National Academy of Sciences of the United States of America.* 2008; 105:21000–21005. [PubMed: 19064919]
- Wingo TL, Shah VN, Anderson ME, Lybrand TP, Chazin WJ, Balsler JR. An EF-hand in the sodium channel couples intracellular calcium to cardiac excitability. *Nature structural & molecular biology.* 2004; 11:219–225.
- Xu W, Lipscombe D. Neuronal Ca(V)1.3 $\alpha$ (1) L-type channels activate at relatively hyperpolarized membrane potentials and are incompletely inhibited by dihydropyridines. *The Journal of neuroscience : the official journal of the Society for Neuroscience.* 2001; 21:5944–5951. [PubMed: 11487617]
- Yamaguchi K, Ohmori H. Voltage-gated and chemically gated ionic channels in the cultured cochlear ganglion neurone of the chick. *The Journal of physiology.* 1990; 420:185–206. [PubMed: 1691290]
- Yamoah EN, Crow T. Two components of calcium currents in the soma of photoreceptors of *Hermisenda*. *Journal of neurophysiology.* 1994; 72:1327–1336. [PubMed: 7807215]
- Yamoah EN, Lumpkin EA, Dumont RA, Smith PJ, Hudspeth AJ, Gillespie PG. Plasma membrane Ca<sup>2+</sup>-ATPase extrudes Ca<sup>2+</sup> from hair cell stereocilia. *The Journal of neuroscience : the official journal of the Society for Neuroscience.* 1998; 18:610–624. [PubMed: 9425003]
- Zampini V, Johnson SL, Franz C, Lawrence ND, Munkner S, Engel J, Knipper M, Magistretti J, Masetto S, Marcotti W. Elementary properties of CaV1.3 Ca(2+) channels expressed in mouse cochlear inner hair cells. *The Journal of physiology.* 2010; 588:187–199. [PubMed: 19917569]
- Zhang XL, Gold MS. Dihydropyridine block of voltage-dependent K<sup>+</sup> currents in rat dorsal root ganglion neurons. *Neuroscience.* 2009; 161:184–194. [PubMed: 19289157]

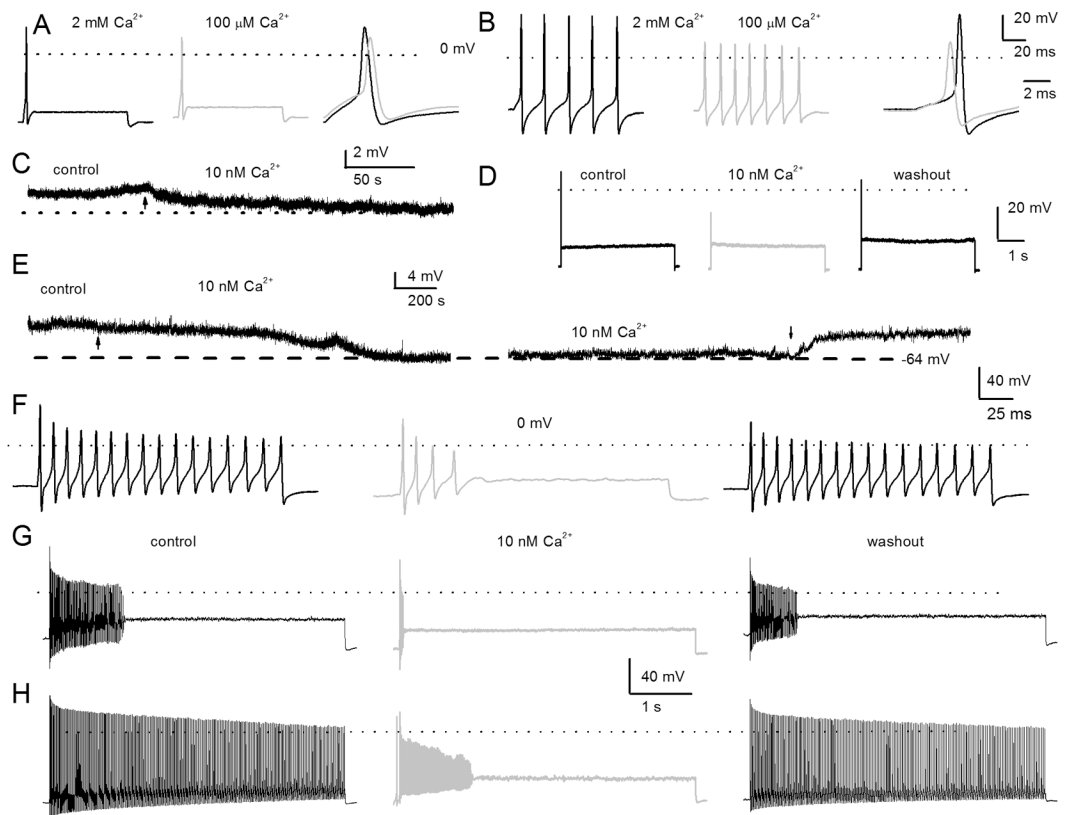


**Figure 1. Effects of changes in external  $\text{Ca}^{2+}$  on action potentials in post-hearing spiral ganglion neurons**

**A** We used the perforated-patch configuration to evoke electrical activity from apical, rapidly adapting spiral ganglion neurons in 2 mM extracellular  $\text{Ca}^{2+}$  (left panel, in black), and after (middle panel, in light gray) bath perfusion of extracellular solution containing  $\sim 100 \mu\text{M}$   $\text{Ca}^{2+}$ . The magnitude and duration of the injected current were 0.2 nA and 100 ms, respectively. On the right panel, we superimposed evoked action potentials recorded in 2 mM  $\text{Ca}^{2+}$  and 100  $\mu\text{M}$   $\text{Ca}^{2+}$ -free solutions. The peaks of the action potentials were (in mV):  $28 \pm 3$  in 2 mM  $\text{Ca}^{2+}$ , and  $10 \pm 6$  in 100  $\mu\text{M}$   $\text{Ca}^{2+}$  bath solutions ( $n = 8$ ;  $p < 0.05$ ), and the maximum right slopes were (mV/ms):  $-99 \pm 16$  in 2 mM  $\text{Ca}^{2+}$ , and  $-78 \pm 4$  in 100  $\mu\text{M}$   $\text{Ca}^{2+}$  bath solution ( $n = 8$ ;  $p < 0.05$ ). **B** Evoked action potentials were elicited with a 0.05 nA current for  $\sim 100$  ms from a basal, slowly adapting, SGN in a bath solution containing 2 mM  $\text{Ca}^{2+}$  (left panel,) and after a bath perfusion of  $\sim 100 \mu\text{M}$   $\text{Ca}^{2+}$  solution (middle panel). The right panel shows a comparison of action potential profiles in the two treatment conditions. The dashed lines show 0 mV levels. The peaks of the action potentials were (in mV):  $37.0 \pm 7$  in 2 mM  $\text{Ca}^{2+}$ , and  $16 \pm 3$  in 100  $\mu\text{M}$   $\text{Ca}^{2+}$  bath solutions ( $n = 9$ ;  $p < 0.05$ ), and the maximum right slopes were (mV/ms):  $-149 \pm 1$  in 2 mM  $\text{Ca}^{2+}$ , and  $-83 \pm 15$  in 100  $\mu\text{M}$   $\text{Ca}^{2+}$  bath solution ( $n = 9$ ;  $p < 0.05$ ). **C** Shown is the characteristic resting membrane potential (rmp) of a 3-month old apical SGN. Reduction of external  $\text{Ca}^{2+}$  from 2 mM to  $\sim 10$  nM produced modest hyperpolarization of the rmp. The summary data show that the rmp for apical neurons was (control)  $-58 \pm 6$  mV and (10 nM  $\text{Ca}^{2+}$ )  $-61 \pm 4$  mV ( $n = 9$ ;  $p = 0.12$ ). The effect of reduced  $\text{Ca}^{2+}$  was reversible after washout with control solution. **D** Injection of 0.2 nA current produced single spikes in apical SGNs. **E** Exemplary current-clamp recordings from SGNs from the basal turn of the cochlea showed the rmp in control solutions and after application of 10 nM  $\text{Ca}^{2+}$ -solution. The effects of 10 nM  $\text{Ca}^{2+}$  solution were reversible. Summary data from 15 basal SGNs show that the rmp in control solution

was:  $-55 \pm 5$  mV and in 10 nM- $\text{Ca}^{2+}$  solution was:  $-64 \pm 3$  mV ( $n = 15$ ;  $p < 0.05$ ). **F–H** The spike frequency of adult basal SGNs was heterogenous. **F–G** show data from the same neuron after injection of 0.2 nA current for ~200 ms (**F**) and ~5 s (**G**), respectively. In 10 nM external  $\text{Ca}^{2+}$ , the spike frequency plummeted by ~5-fold compared to control (from  $17 \pm 7$  Hz (control) to  $3 \pm 2$  Hz (10 nM  $\text{Ca}^{2+}$ ;  $n = 9$ ;  $p < 0.05$ ). Upon washout the spike frequency was restored to  $12 \pm 7$  Hz ( $n = 9$ ;  $p = 0.08$ ). **H** In slowly adapting SGNs that fire unabatedly after injecting 0.2 nA for 5 s, the spike frequency was reduced by ~4-fold after application of 10 nM-  $\text{Ca}^{2+}$ solutions. From control to 10-nM  $\text{Ca}^{2+}$  solution the spike frequency changed from  $49 \pm 10$  Hz (control) to  $12 \pm 6$  Hz (10-nM  $\text{Ca}^{2+}$ ;  $n = 11$ ;  $p < 0.05$ ). The firing frequency after washout was  $39 \pm 14$  Hz ( $n = 11$ ;  $p = 0.11$ ).

\$watermark-text

\$watermark-text

\$watermark-text



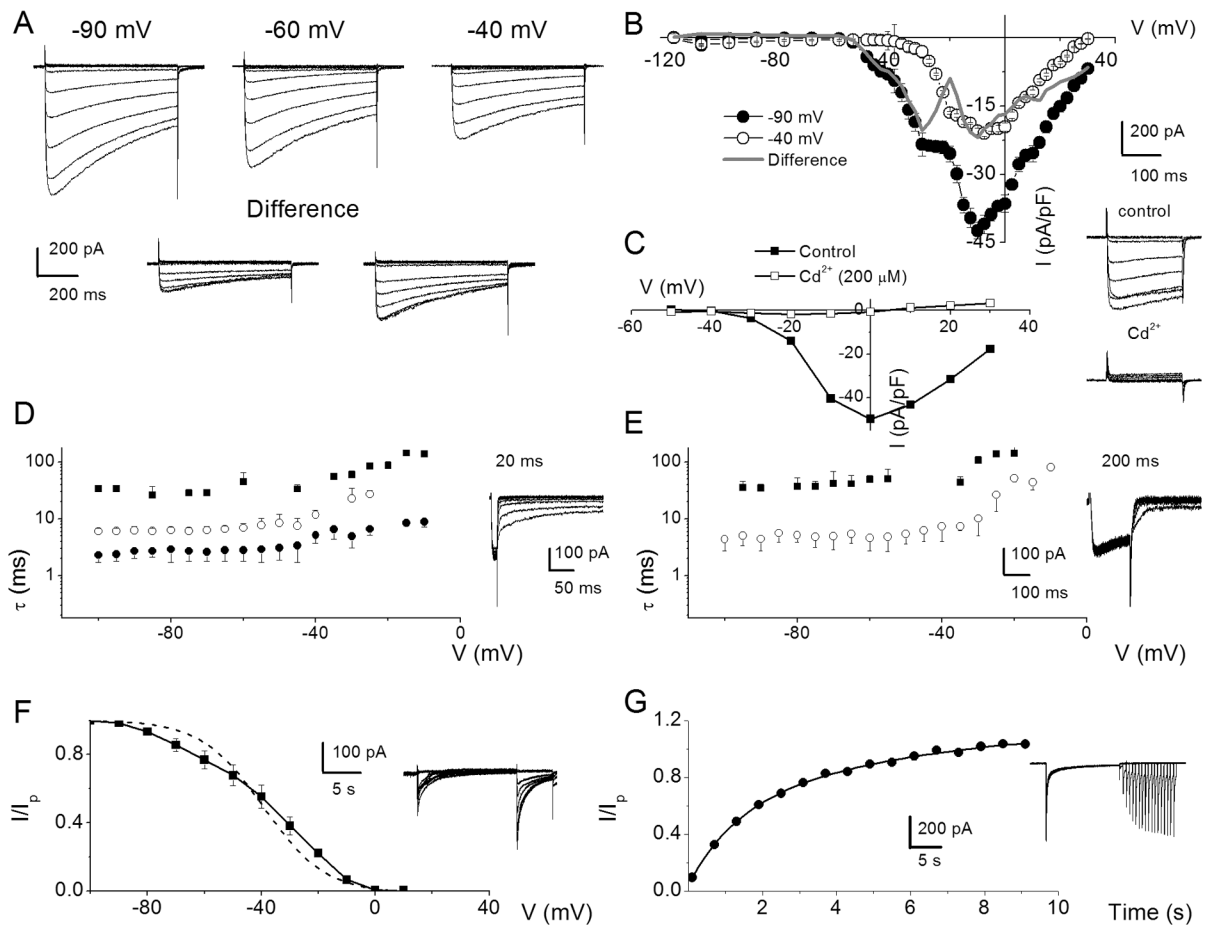


**Figure 2. Whole-cell  $\text{Ca}^{2+}$  currents in SGNs may contain several components**

**A** A family of membrane  $\text{Ca}^{2+}$  current traces recorded from SGNs using 5 mM external  $\text{Ca}^{2+}$ . Inward  $\text{Ca}^{2+}$  currents were generated using depolarizing test voltages from  $-120$  to  $30$  mV in  $2.5 - 10$  mV increments from a holding voltage of  $-90$  mV. Current traces recorded from the same neuron from a holding voltage of  $-60$  and  $-40$  mV. The difference between current traces recorded at  $-90$  and  $-60$  mV (inset, left panel) and  $-90$  and  $-40$  mV (inset, right panel) holding voltages. **B** Summary of the corresponding current-density-voltage ( $I-V$ ) relations for recordings at  $-90$  (●) and  $-40$  (○) mV holding voltages together with the difference (difference between currents at  $-90$  and  $-40$  mV) current densities is shown in the gray line. Data were summarized from  $n = 15$ . **C** A family of control current traces generated from a holding voltage of  $-70$  mV. (inset right panel). After application of  $\text{Cd}^{2+}$  ( $200 \mu\text{M}$ ), the whole-cell  $\text{Ca}^{2+}$  current was blocked (inset as indicated). The corresponding  $I-V$  relations are shown (control in ■, and  $\text{Cd}^{2+}$  in □). **D** SGNs were held at  $-80$  mV and  $\text{Ca}^{2+}$  currents were elicited for 20 ms to 10 mV. At the end of the pre-pulse, the membrane voltage was polarized to different test voltages in 5-mV increments (between  $-100$  and  $-5$  mV), and the kinetics of the tail currents were examined. **E** A similar protocol was applied using a 200-ms pre-pulse. The current traces are shown as insets. Summary data of the relations between the time constant of deactivation (■, ●, ○) and test voltages using 20-ms (**D**) and 200-ms (**E**) pre-pulses ( $n = 10$ ). Invariably, multiple deactivation time constants were documented using shorter pre-pulse voltages. Three time constants were derived using 20-ms pre-pulse. In contrast, two time constants best fitted the deactivation kinetics using 200-ms pre-pulse. **F** Exemplary current traces elicited to generate steady-state inactivation

curves depicted in inset. The neuron was held at  $-70$  mV and stepped to conditioning voltages varying from  $-100$  to  $40$  mV for  $\sim 15$  s, followed by a test voltage at  $10$  mV. The current was normalized against the non-inactivating component evoked at the test voltage. The dotted curve represents a first order Boltzmann function fit. However, the data was best fitted with a second order Boltzmann function, in solid line. The half-inactivation voltages ( $V_{1/2-1}$ , mV) were  $-65 \pm 8$  (at  $\sim 35\%$  contribution) and ( $V_{1/2-2}$ )  $-32 \pm 3$  (at  $\sim 65\%$  contribution) ( $n = 9$ ) and the maximum slope factors ( $k$ , in mV) were  $9.0 \pm 1$  and  $10 \pm 2$ . ( $n = 9$ ). **G** Neurons were held at  $-80$  mV and stepped to conditioning pre-pulse ( $10$  mV) to make a transition from activation to inactivation. Subsequently, test pulses at varying time intervals were applied. The traces shown as inset are a family of currents obtained after applying a set of pulses as described. The currents elicited at the test pulse at specific times after the conditioning pre-pulse were normalized against conditioning pulse-evoked current and plotted against time. At least two time constants ( $\tau$ ) of recovery from inactivation were obtained:  $\tau_1 = 1.3 \pm 0.2$  s and  $\tau_2 = 7.2 \pm 1.6$  s ( $n = 11$ ).

\$watermark-text

\$watermark-text

\$watermark-text

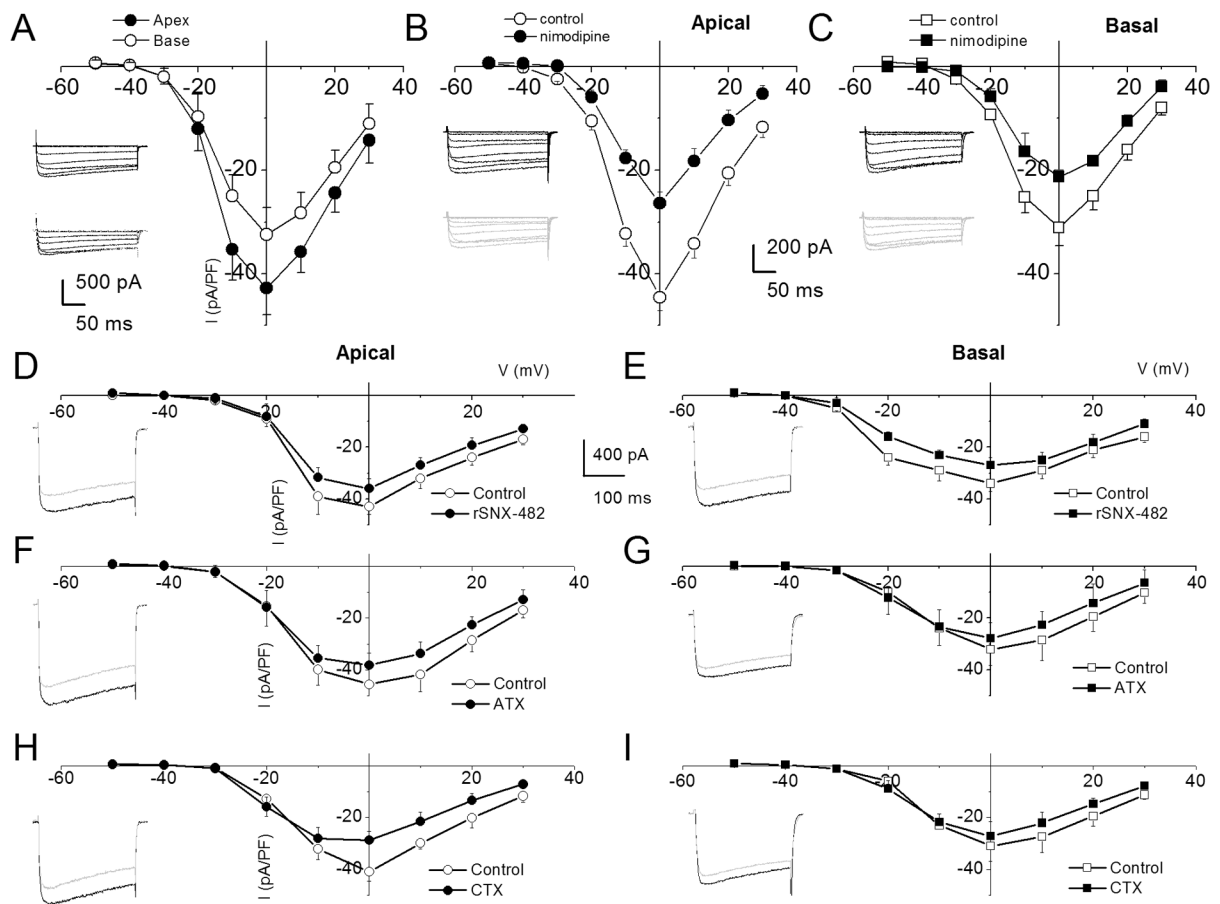


**Figure 3. Characteristics of  $\text{Ca}^{2+}$  currents in 3-month old spiral ganglion neurons from apical and basal turns of the cochlea, and the effects of  $\text{Ca}^{2+}$  current blockers**

**A** Family of inward  $\text{Ca}^{2+}$  currents from apical SGN elicited from a holding potential of  $-70$  mV to step potentials from  $-50$  to  $30$  mV in  $10$ -mV increments, (inset at the left panel). A similar voltage pulse protocol was applied to generate  $\text{Ca}^{2+}$  current traces from basal SGNs (inset at the right panel). Peak  $\text{Ca}^{2+}$  current density-voltage relations for apical (●) and basal (○) SGNs. At voltages ( $-10$  to  $10$  mV), there were significant differences between apical and basal  $\text{Ca}^{2+}$  current-densities ( $* = p < 0.05$ ;  $n = 17$ ). **B** The dihydropyridine antagonist, nimodipine, blocks a component of whole cell  $\text{Ca}^{2+}$  currents in SGNs. Current traces recorded from neurons isolated from apical (inset, upper (control) and lower (nimodipine) panels) segments of the cochlea. Perfusion of external solution containing  $10$   $\mu\text{M}$  nimodipine resulted in a reduction of the  $\text{Ca}^{2+}$  currents. The corresponding current density-voltage relations for apical (**B**) and basal (**C**) SGNs ( $n = 9$ ). The control data is illustrated with black lines and symbols and the residual current after nimodipine block is shown in blue lines and symbols. **D** The current-density-voltage relations were generated before (in black lines and symbols) and after (in blue lines and symbols) application of  $\text{Ca}^{2+}$  current blockers, rSNX-482, for R-type (**D–E**),  $\omega$ -Agatoxin IVA (ATX), for P/Q-type (**F–G**), and  $\omega$ -Conotoxin MVIIA (CTX) for N-type (**H–I**) currents. **D–E** Shown are the current-density-voltage relations for control (in black) and the remaining current-density after application of toxins (in blue) for apical (**D**) and basal (**E**) SGNs ( $n = 6$ ). The insets on the left panels of the plots are representative current traces recorded from a holding voltage of  $-70$  mV to a step voltage of  $0$  mV. **F–G** Similar data obtained upon recording control  $\text{Ca}^{2+}$  currents and after application of the P/Q-type  $\text{Ca}^{2+}$  current blocker,  $1$   $\mu\text{M}$   $\omega$ -Agatoxin IVA

(ATX). **H–I** Summary data of the effects of the N-type  $\text{Ca}^{2+}$  channel blocker, on apical versus basal neurons. Table 1 illustrates the summary data for the effects of  $\text{Ca}^{2+}$  channel blockers on whole-cell  $\text{Ca}^{2+}$  currents.

\$watermark-text

\$watermark-text

\$watermark-text

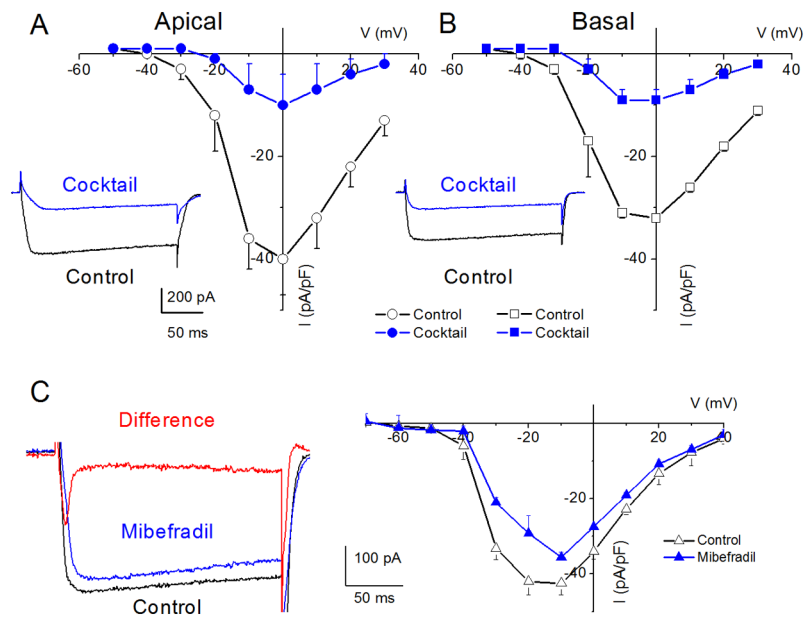


**Figure 4. Whole-cell  $\text{Ca}^{2+}$  currents in SGNs resistant to a cocktail of L-, N-, P/Q-, and R-type current blockers and mibefradil-sensitive currents**

A cocktail of  $10 \mu\text{M}$  nimodipine,  $1 \mu\text{M}$   $\omega$ -agatoxin IVA,  $1 \mu\text{M}$  conotoxin MVIIA, and  $200 \text{ nM}$  rSNX-482 was used. **A** Current traces recorded using a holding voltage of  $-70$  to a step voltage of  $0$  mV in apical neurons (control current trace in black and after application of blocker cocktail in blue). **B** Similar data obtained from basal neurons as described in **A**. The corresponding current-density voltage relations for apical (**A**) and basal (**B**) neurons ( $n = 7$ ). The cocktail blocked  $81.6 \pm 7.8\%$  ( $n = 7$ ) of the total  $\text{Ca}^{2+}$  currents' in apical neurons. Meanwhile  $71.1 \pm 6.2\%$  ( $n = 7$ ) of the total  $\text{Ca}^{2+}$  currents were blocked in basal neurons. **C**  $\text{Ca}^{2+}$  current traces from a basal SGN held at a holding potential of  $-90$  mV and stepped to  $-10$  mV. The control trace (in black) and the residual current after application of  $5 \mu\text{M}$  mibefradil (in blue) are shown. The difference current or the mibefradil-sensitive current shows a transient profile, consistent with T-type  $\text{Ca}^{2+}$  currents (in red). The corresponding current-voltage relations are shown from data from four basal SGNs.



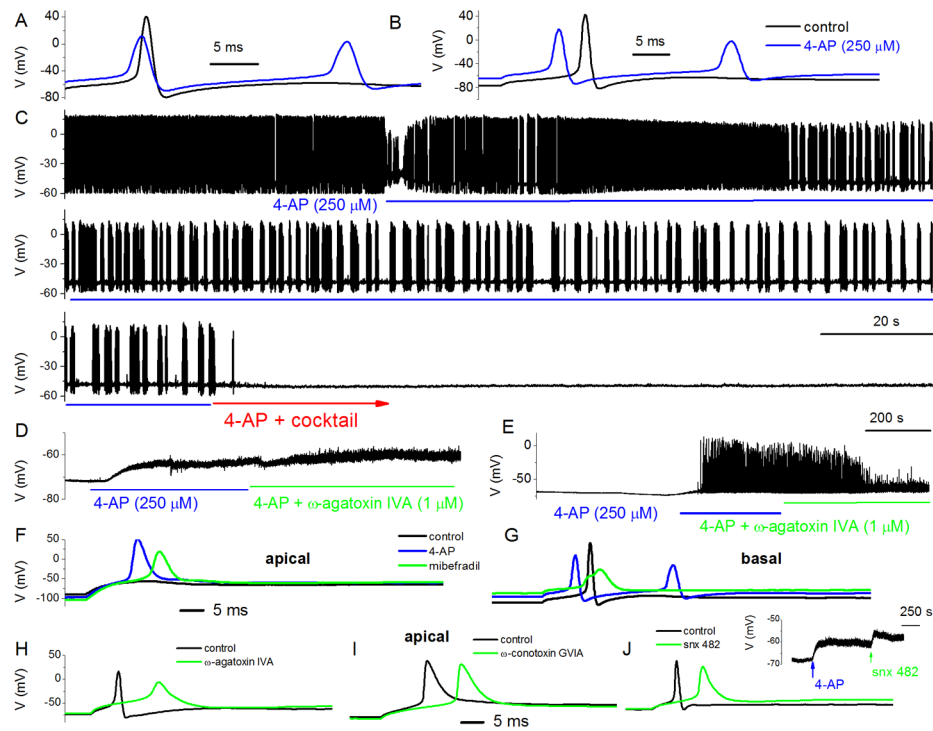


**Figure 5. Effects of 4-AP and  $\text{Ca}^{2+}$  current blockers on membrane properties of adult SGNs**  
 To enhance and resolve the effects of  $\text{Ca}^{2+}$  current blockers on action potentials in SGNs, we used 4-AP (250  $\mu\text{M}$ ) to broaden the action potentials. **A** Evoked action potentials (0.2 nA current) recorded from a 3-month-old basal SGN, before and after application of bath solution containing 250  $\mu\text{M}$  4-AP. **B** Rebound action potentials following injection of negative current ( $-0.5$  nA). **C** In spontaneously active SGNs, 4-AP altered the firing pattern. Upon application of bath solution containing 4-AP and a cocktail of  $\text{Ca}^{2+}$  current blockers (10  $\mu\text{M}$  nimodipine for L-type, 1  $\mu\text{M}$   $\omega$ -Agatoxin IVA (ATX) for P/Q-, 1  $\mu\text{M}$   $\omega$ -Conotoxin MVIIA (CTX) for N-, 200 nM rSNX-482 for R-, and 5  $\mu\text{M}$  mibefradil for T-type currents), spontaneous activity was attenuated. **D** Besides alteration of the shape and firing patterns of action potentials, 250  $\mu\text{M}$  4-AP was sufficient to produce substantial depolarization of SGNs (rmp for control  $-65 \pm 9$  mV after application of 4-AP,  $-61 \pm 7$  mV ( $n = 8$ )). Blockade of P/Q-type  $\text{Ca}^{2+}$  currents with 1  $\mu\text{M}$   $\omega$ -Agatoxin IVA resulted in small but consistent depolarization of the rmp (controls =  $-64 \pm 8$  mV after  $\omega$ -Agatoxin =  $-57 \pm 2$  mV ( $n = 8$ )). **E** In six out of ten SGNs 4-AP-induced-depolarization triggered spontaneous activity. Suppression of P/Q-type  $\text{Ca}^{2+}$  currents reduced the spike amplitude and frequency (five out of six SGNs). **F** Adult apical SGNs was injected with  $-0.5$  nA, and slight rebound depolarization followed (in black trace). Upon application of 250  $\mu\text{M}$  4-AP solution, injection of  $-0.5$  nA sufficed to elicit rebound action potential (in red). Shown in green trace is the resulting action potential after application of bath solution containing 250  $\mu\text{M}$  4-AP and 5  $\mu\text{M}$  mibefradil. **G** Similar but not identical data obtained from age-matched basal SGNs. **H** The resulting effects of blockade of P/Q-type current (control in black and after 4-AP and toxin in green traces) in apical SGNs. The 4-AP-mediated traces were omitted for clarity but see Table 2. **I & J** Changes in action potential properties following inhibition of N- and R- type  $\text{Ca}^{2+}$  currents, respectively. Shown in the inset is the effect of 4-AP and the R-type channel blocker on the rmp. Table 2 outlines the summary data from both apical and basal SGNs.

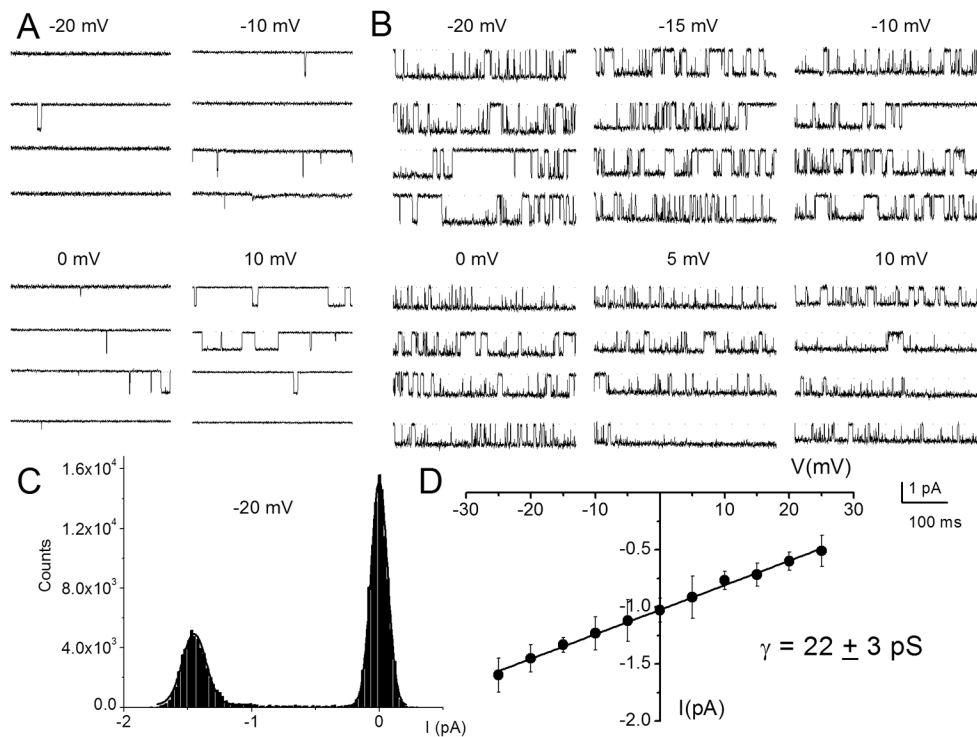


**Figure 6. Effects of dihydropyridine  $\text{Ca}^{2+}$  channel agonist, Bay K 8644 on single-channel  $\text{Ca}^{2+}$  currents**

**A** Single-channel  $\text{Ba}^{2+}$  current traces were recorded in the cell-attached mode using 50 mM  $\text{Ba}^{2+}$  as the charge carrier. The traces were generated by holding the membrane patch at  $-70$  mV and stepped to potentials indicated above each set of traces. The continuous dotted lines indicate the closed level and the downward steps indicate the opened level. Brief openings were more frequent than long openings in the unmodified channel. **B** Illustration of the effects of  $5 \mu\text{M}$  Bay K 8644 on the same patch as it is shown in **A**. Bay K 8644 promoted long openings. Whereas Bay K 8644 increased the frequency and duration of single-channel openings, nimodipine ( $10 \mu\text{M}$ ) had the opposite effect (data not shown). **C** An example of amplitude histogram used to determine the mean magnitude of unitary currents at different step potential is shown. **D** Single-channel conductance ( $\bullet$ ) of L-type channel for  $\text{Ba}^{2+}$  was determined using linear least square fits to the mean single-channel amplitude at different step potentials. The conductance of the L-type channel was  $22 \pm 3$  pS ( $n = 11$ ).

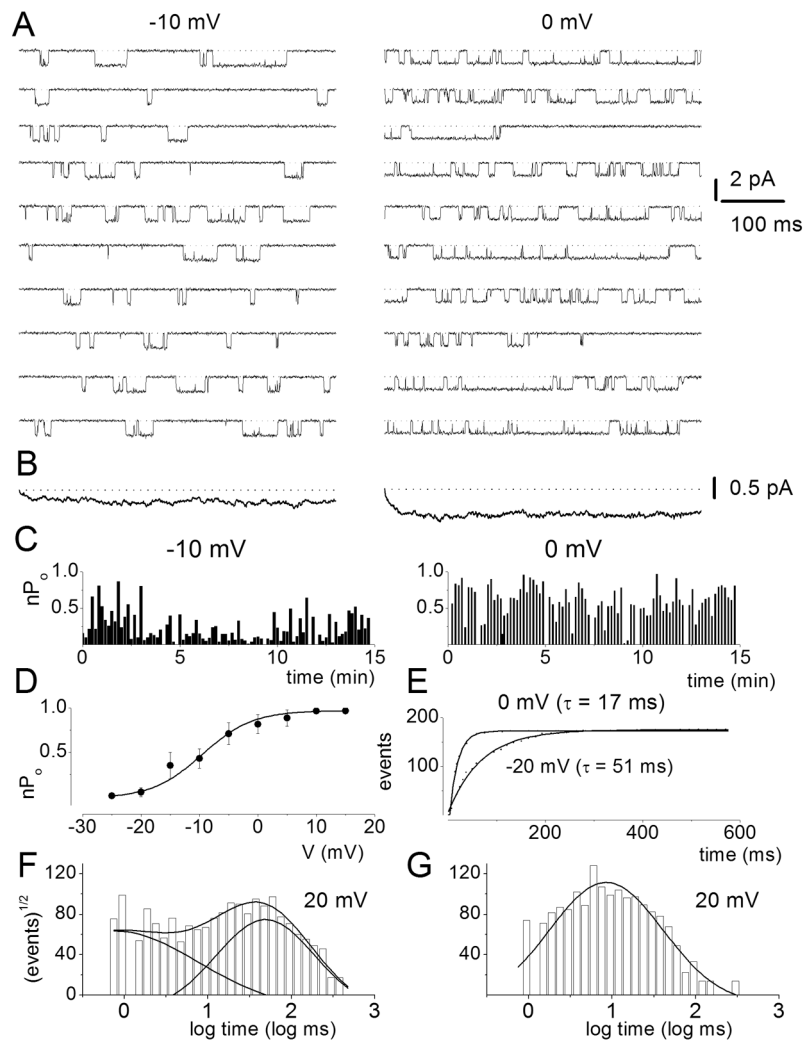


**Figure 7. Voltage-dependence of L-type single-channel currents in adult spiral ganglion neurons**  
**A** Representative consecutive single-channel traces of  $Ba^{2+}$  currents at test potentials  $-10$  and  $0$  mV were obtained from L-type channel using the agonist, Bay K 8644 ( $5\mu M$ ) in the bath solution. Ten consecutive traces are shown at the step potentials indicated, from a holding potential of  $-70$  mV. **B** Ensemble-averaged currents at a given test potential were constructed from idealized current traces from  $\sim 400$  consecutive sweeps. The ensemble-averaged current traces derived are shown at the bottom of each column of traces. **C** Diary of the channel open probability ( $P_o$ ) at test potentials of  $-10$  and  $0$  mV are shown.  $P_o$  versus voltage relation for L-type channels were obtained from 500-ms voltage steps ranging from  $-25$  to  $15$  mV. Each symbol represents the mean  $P_o$  (including null traces) determined from 400 consecutive sweeps. The continuous solid line represents a single Boltzmann function fit to the data points. The half-activation voltage ( $V_{1/2}$ ) was  $-9.5 \pm 2.4$  mV ( $n = 7$ ) and the slope was e-fold for  $4.3 \pm 1.2$  mV ( $n = 7$ ). **E** Voltage-dependence of first latency distribution in single-channel  $Ba^{2+}$  currents is shown. Cumulative first latency distribution plots were generated from the waiting time to first opening as a function of time, at the step voltages indicated. Exponential fits to the first latency distribution are drawn with solid lines. Time constants of the first latency distribution ( $\tau$ ) are indicated. **F–G** Dwell time histograms were binned logarithmically using 10 bins per decade and plotted with a square root transformation of the number of events. Open (**F**) and closed time (**G**) distribution were

fitted with two open ( $\tau_{o1}$  and  $\tau_{o2}$ ) and two closed ( $\tau_{c1}$  and  $\tau_{c2}$ ) time constants, respectively. However, at some step voltages as shown (20 mV), the fast closed dwell time constant could not be resolved. For example at 0 mV step voltage  $\tau_{o1} = 1.7 \pm 0.6$  ms ( $n = 5$ ) and  $\tau_{o2} = 37.0 \pm 6.1$  ms ( $n = 5$ ) and  $\tau_{c1} = 0.6 \pm 0.1$  ms ( $n = 5$ ) and  $\tau_{c2} = 13.2 \pm 4.7$  ms ( $n = 5$ ). Moreover, at 20 mV step voltage as shown  $\tau_{o1} = 0.8 \pm 0.3$  ms ( $n = 6$ ) [17%] and  $\tau_{o2} = 48.0 \pm 6$  ms ( $n = 6$ ) [83%], and  $\tau_c = 8.5 \pm 1.2$  ms ( $n = 6$ ). The numbers in parentheses represent the percentage of time in which the channel dwells at the different states.

\$watermark-text

\$watermark-text

\$watermark-text

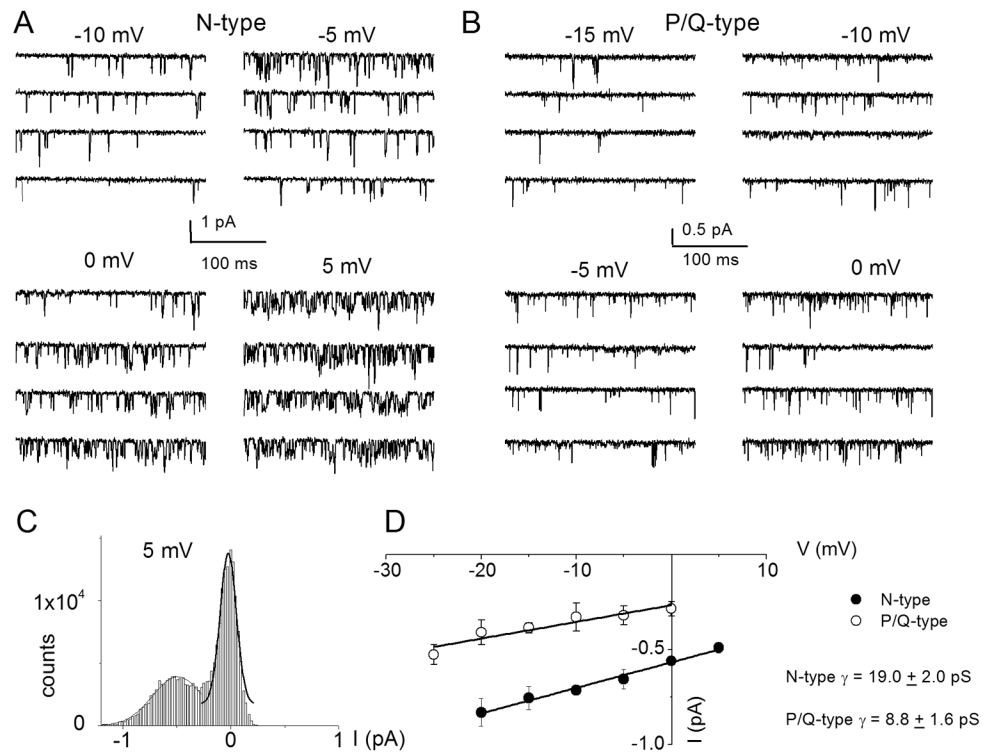


**Figure 8. Single-channel recordings of N- and P/Q-type channels in spiral ganglion neurons**  
**A** Inward  $\text{Ba}^{2+}$  currents through single  $\text{Ca}^{2+}$  channels were recorded in membrane patches from isolated 3-month old SGNs. For recordings of N-type single channel activity, we included a cocktail of  $\text{Ca}^{2+}$  channel blockers containing: 10  $\mu\text{M}$  nimodipine, 1  $\mu\text{M}$   $\omega$ -agatoxin IVA, 200 nM  $\omega$ -(rSNX-482) and 5  $\mu\text{M}$  mibefradil in the external and patch-electrode solutions. The membrane patch was held at  $-70$  mV and stepped to test voltages indicated above each set of four consecutive traces. The solid dotted lines denote the closed levels. The test potential for the example shown is 5 mV. **C** Representative current-voltage ( $I$ - $V$ ) plots for N-type channels show single-channel conductance of  $19 \pm 2$  pS ( $n = 7$ ). **B** To record the unitary P/Q-type single channel fluctuations, we included a cocktail of  $\text{Ca}^{2+}$  channel blockers containing: 10  $\mu\text{M}$  nimodipine, 1  $\mu\text{M}$  conotoxin MVIIA, 200 nM  $\omega$ -(rSNX-482) and 5  $\mu\text{M}$  mibefradil in the external and patch-electrode solutions. Under outside-out cell-attached configuration, 3-month old SGNs membrane patches were held at  $-70$  mV and stepped to the depolarizing potentials, indicated beside the family of consecutive traces. We used 50 mM  $\text{Ba}^{2+}$  as the charge carrier. **C** The amplitude histogram from current traces at 5 mV step potential is shown. Similar data were used to generate the unitary current amplitude-voltage ( $I$ - $V$ ) plots. **D** The scattered points of the  $I$ - $V$  relation were fitted with a linear regression to determine the conductance of the P/Q channels. For the summary data shown, the single channel conductance ( $\gamma$ ) values for P/Q-type channels in 50 mM  $\text{Ba}^{2+}$  is (in pS):  $8.8 \pm 1.6$  pS ( $n = 6$ ).



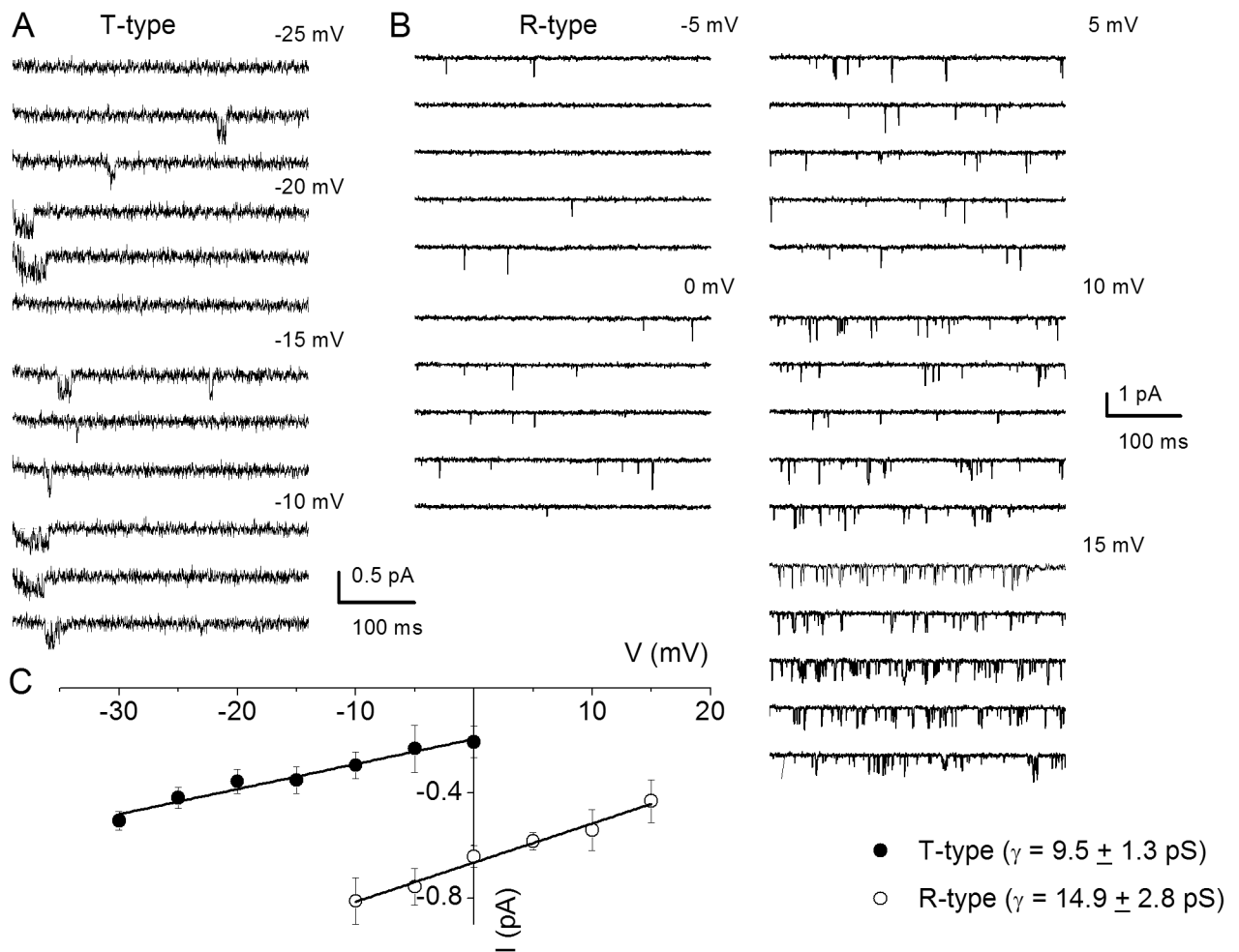


**Figure 9. Single-channel conductance of T- and R-type  $\text{Ca}^{2+}$  channels in adult spiral ganglion neurons**

**A** Representative and consecutive single-channel traces recorded in a cell-attached patch with pipette solution containing 50 mM  $\text{Ba}^{2+}$ . Additionally, the patch-pipette and bath solution consisted of a cocktail of  $\text{Ca}^{2+}$  channel blockers; 10  $\mu\text{M}$  nimodipine, 1  $\mu\text{M}$  conotoxin MVIIA, 200 nM  $\omega$ -(rSNX-482) and 1  $\mu\text{M}$   $\omega$ -agatoxin IVA. The holding potential was  $-90$  mV and the step potentials are indicated. **B** To examine the unitary current fluctuations of R-type  $\text{Ca}^{2+}$  channels, we included a cocktail of  $\text{Ca}^{2+}$  channel blockers containing: 10  $\mu\text{M}$  nimodipine, 1  $\mu\text{M}$  conotoxin MVIIA, 5  $\mu\text{M}$  mibefradil and 1  $\mu\text{M}$   $\omega$ -agatoxin IVA in the bath and pipette solutions. Shown are sets of families of consecutive single-channel sweeps recorded in the cell-attached configuration, using 50 mM  $\text{Ba}^{2+}$  as the charge carrier. The membrane patch was held at a holding potential of  $-70$  mV and stepped to potentials denoted above each set of sweeps. **C** The  $I$   $V$  relationships are shown for T and R-type unitary currents, respectively. The single-channel conductances were: T-type  $9.5 \pm 1.3$  pS ( $n = 5$ ) and R-type channels  $14.9 \pm 2.8$  pS ( $n = 6$ ).

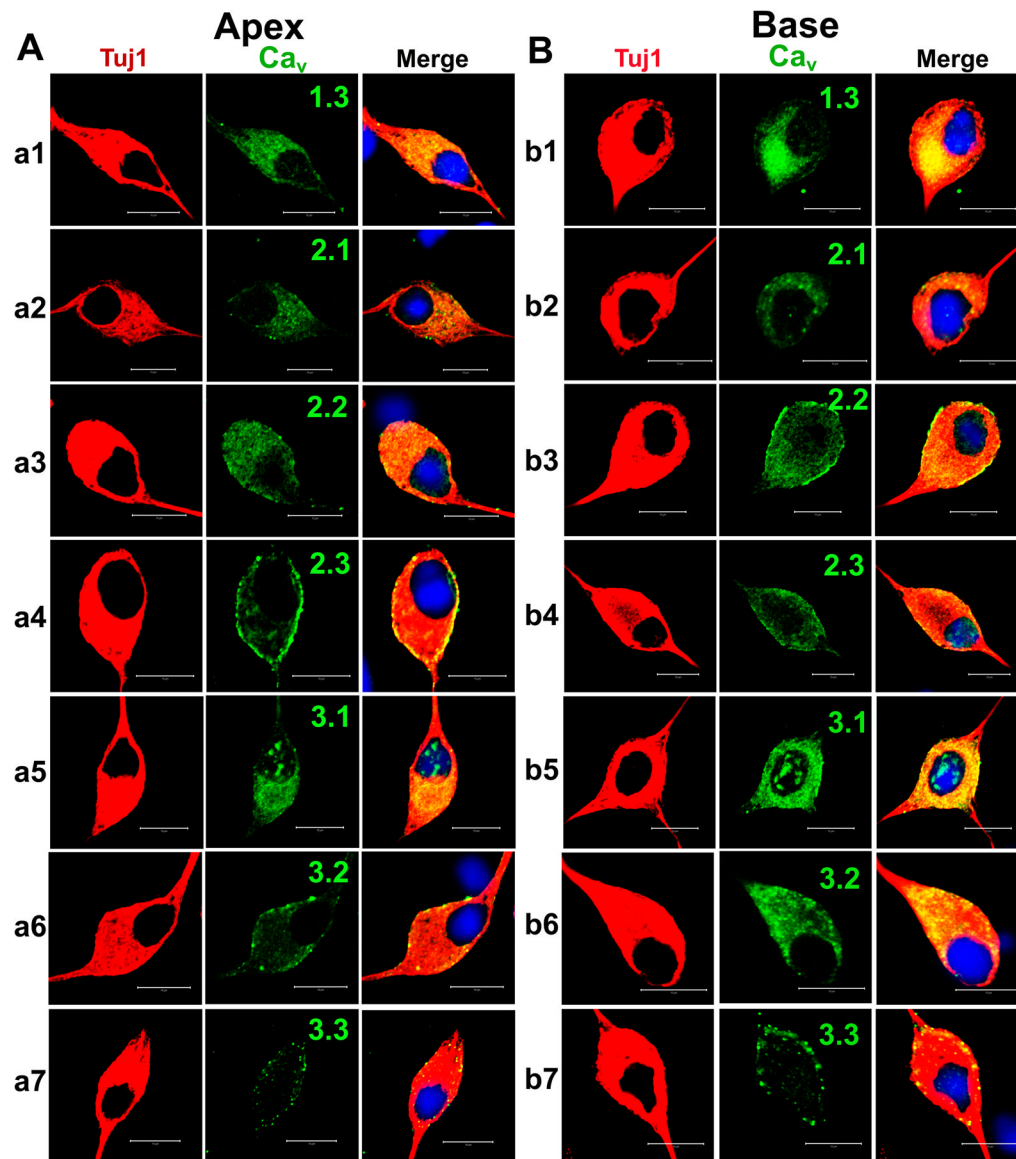


**Figure 10. Cultured spiral ganglion neurons express multiple Ca<sup>2+</sup> channels**

**A** Cultured (48 hrs in culture) apical spiral ganglion neurons were fixed and labeled with antibodies against Ca<sub>v</sub>1.3, Ca<sub>v</sub>2.1, Ca<sub>v</sub>2.2, Ca<sub>v</sub>2.3, Ca<sub>v</sub>3.1, Ca<sub>v</sub>3.2, and Ca<sub>v</sub>3.3. As shown, neurons were labeled with the neuronal marker Tuj1 (in red, left panels, a<sub>1</sub>–a<sub>7</sub>), the channels (in green, middle left panel), and the nuclei were stained with DAPI (in blue) and the merged images (right panel). Spiral ganglion neurons stained positively for Ca<sub>v</sub>1.3, Ca<sub>v</sub>2.1, Ca<sub>v</sub>2.2, Ca<sub>v</sub>2.3, Ca<sub>v</sub>3.1, Ca<sub>v</sub>3.2, and Ca<sub>v</sub>3.3. **B** Similar data were obtained for basal neurons as shown in b<sub>1</sub>–b<sub>7</sub> for Tuj1, nuclei stain and channels Ca<sub>v</sub>1.3, Ca<sub>v</sub>2.1, Ca<sub>v</sub>2.2, Ca<sub>v</sub>2.3, Ca<sub>v</sub>3.1, Ca<sub>v</sub>3.2, and Ca<sub>v</sub>3.3, respectively. Scale bar = 10 μm.

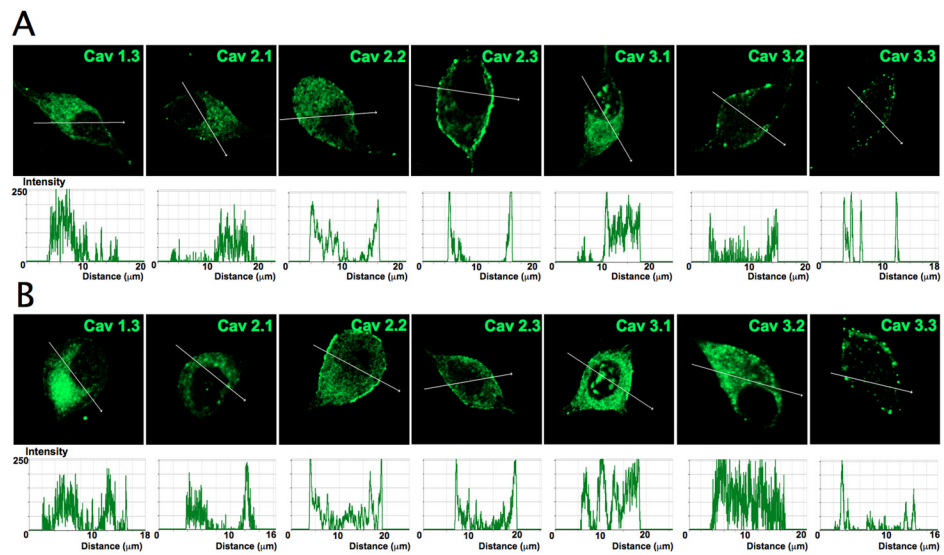


**Figure 11. Profile of  $\text{Ca}^{2+}$  channel expression in plasma membrane and cytosol of adult spiral ganglion neurons**

To gauge the membrane expression of  $\text{Ca}^{2+}$  channels in SGNs we assembled data from Figure 10 and plotted fluorescent intensity with respective distance across the diameter of neurons. **A** Expression pattern of  $\text{Ca}^{2+}$  channels in apical neurons and **B** basal neurons. Scale bar = 10  $\mu\text{m}$ .

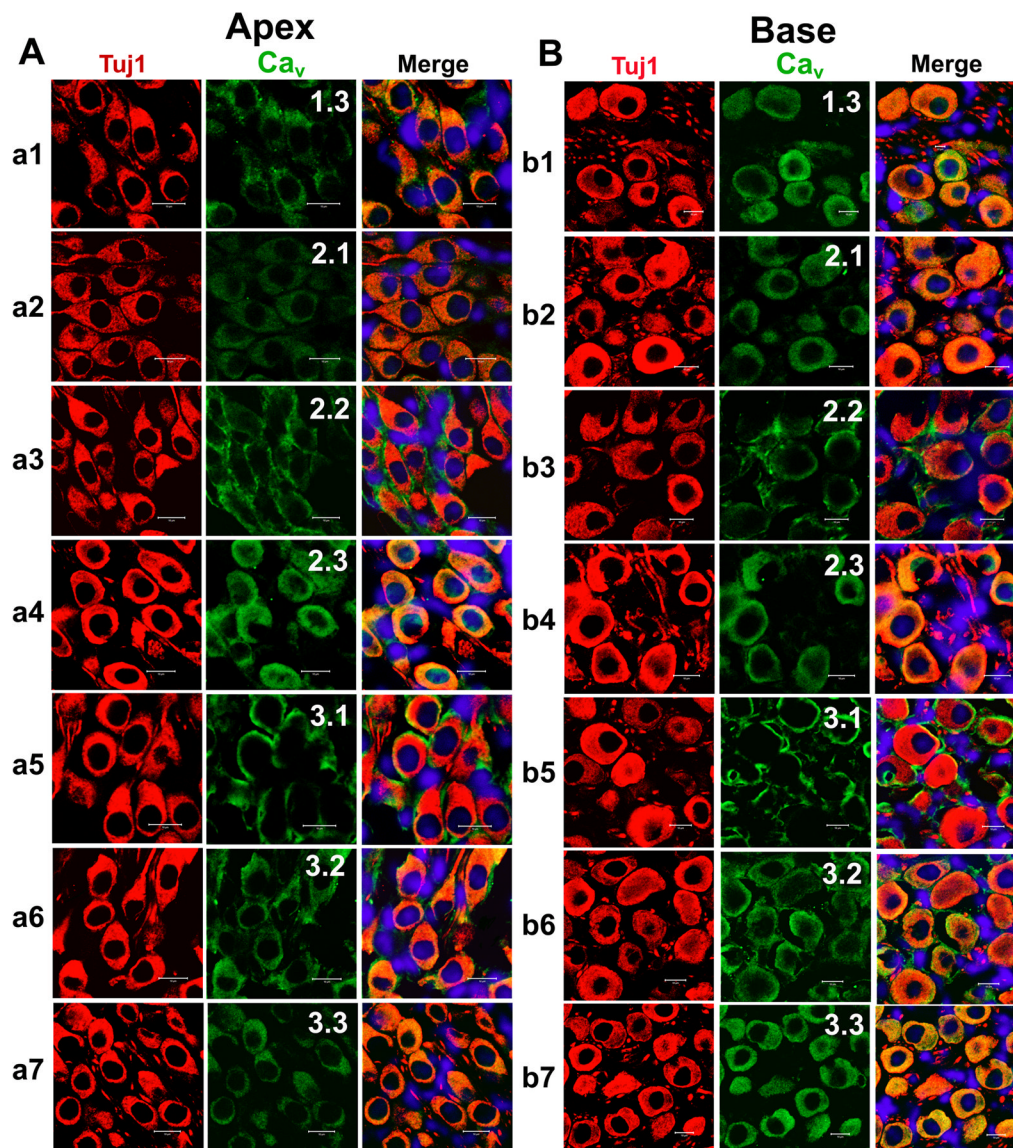


**Figure 12. Expression of Ca<sub>v</sub>1.3, Ca<sub>v</sub>2.1, Ca<sub>v</sub>2.2, Ca<sub>v</sub>2.3, Ca<sub>v</sub>3.1, Ca<sub>v</sub>3.2, and Ca<sub>v</sub>3.3 in mouse cochlea sections**

**A–B.** To rule out the possibility that both apical (**A**) and basal (**B**) SGNs expressed Ca<sup>2+</sup> channels *in vivo* when compared to the cell culture-induced expression of channels, we performed immunolabeling as described in Figure 10 on sections of the cochlea from a 3-month-old mice. Apical spiral ganglion neurons were labeled with antibodies against Ca<sub>v</sub>1.3, Ca<sub>v</sub>2.1, Ca<sub>v</sub>2.2, Ca<sub>v</sub>2.3, Ca<sub>v</sub>3.1, Ca<sub>v</sub>3.2, and Ca<sub>v</sub>3.3. As shown, neurons were labeled with the neuronal marker TuJ1 (in red), the channels (in green), and the nuclei were stained with DAPI (in blue) and the merged images (right panel). Spiral ganglion neurons stained positively to Ca<sub>v</sub>1.3, Ca<sub>v</sub>2.1, Ca<sub>v</sub>2.2, Ca<sub>v</sub>2.3, Ca<sub>v</sub>3.1, Ca<sub>v</sub>3.2, and Ca<sub>v</sub>3.3. **B** Similar data were obtained for basal neurons as shown for Ca<sub>v</sub>1.3, Ca<sub>v</sub>2.1, Ca<sub>v</sub>2.2, Ca<sub>v</sub>2.3, Ca<sub>v</sub>3.1, Ca<sub>v</sub>3.2, and Ca<sub>v</sub>3.3, respectively. Scale bar = 10 μm.

Watermark-text

Watermark-text

Watermark-text

**Table 1**

Percentage of Ca<sup>2+</sup> current blocked by different blockers at 0 mV step voltage

|      | L-type Nimodipine 10 μM | P/Q-type ω-Agatoxin IVA 1 μM | N-type ω-Conotoxin MVIIA 1 μM | R-type rSNX-482 200 nM | Total       |
|------|-------------------------|------------------------------|-------------------------------|------------------------|-------------|
| Apex | 41.0 ± 4.5%             | 17.2 ± 2.7%                  | 22.6 ± 4.3%                   | 15.9 ± 5.7%            | 81.6 ± 7.8% |
| Base | 31.2 ± 2.9%*            | 11.5 ± 5.9%                  | 12.6 ± 2.3%*                  | 19.5 ± 5.1%            | 71.1 ± 6.2% |

\* p<0.05 (apex vs. base) (n = 6)

Table 2

Effects of Ca<sup>2+</sup> current blockers on action potentials

| Apex               | latency (ms) | amplitude (mV) | width (ms)  | Base    | latency (ms) | amplitude (mV) | width (ms)   |
|--------------------|--------------|----------------|-------------|---------|--------------|----------------|--------------|
| Control (n = 7)    | 3.2 ± 1.4    | 93 ± 6         | 1.8 ± 0.4   | (n = 6) | 8.4 ± 1.4    | 111 ± 10       | 9.2 ± 1.4    |
| 4-AP               | 3.0 ± 0.7    | 54 ± 11        | 3.8 ± 0.5   |         | 6.5 ± 0.7    | 78 ± 12*       | 11.6 ± 1.5   |
| 4-AP + mibefradil  | 3.5 ± 1.1    | 39 ± 9**       | 5.2 ± 0.9*  |         | 13.5 ± 2.6*  | 46 ± 15**      | 18.5 ± 1.8** |
| Control (n = 8)    | 4.1 ± 1.2    | 94 ± 8         | 1.9 ± 0.4   | (n = 8) | 9.3 ± 0.9    | 107 ± 12       | 8.8 ± 1.6    |
| 4-AP               | 3.9 ± 1.5    | 71 ± 5         | 3.6 ± 0.3   |         | 6.7 ± 1.1    | 81 ± 9         | 10.2 ± 0.5   |
| 4-AP + rSNX        | 7.0 ± 2.0*   | 67 ± 10*       | 6.2 ± 0.3** |         | 3.4 ± 0.4*   | 68 ± 16**      | 16 ± 1.4*    |
| Control (n = 6)    | 4.4 ± 1.6    | 105 ± 13       | 1.8 ± 0.6   | (n = 5) | 9.5 ± 1.8    | 110 ± 12       | 8.6 ± 1.4    |
| 4-AP               | 3.9 ± 1.1    | 78 ± 12        | 2.9 ± 0.5   |         | 9.9 ± 2.3    | 86 ± 16        | 10.4 ± 1.6   |
| 4-AP + ω-Agatoxin  | 9.1 ± 2.3*   | 43 ± 10**      | 10 ± 1.5**  |         | 5.1 ± 0.5*   | 57 ± 14**      | 18.9 ± 2.2** |
| Control (n = 7)    | 3.7 ± 1.3    | 97 ± 7         | 2.0 ± 0.3   | (n = 7) | 8.2 ± 1.3    | 105 ± 15       | 7.9 ± 1.5    |
| 4-AP               | 3.2 ± 1.1    | 82 ± 16        | 3.2 ± 1.4   |         | 7.1 ± 1.5    | 89 ± 16        | 9.1 ± 2.1    |
| 4-AP + ω-Conotoxin | 7.4 ± 1.3*   | 78 ± 20        | 4.1 ± 1.5   |         | 11.8 ± 0.5*  | 85 ± 20        | 12 ± 4.4     |
| Control (n = 8)    | 4.0 ± 1.6    | 101 ± 14       | 1.7 ± 0.5   | (n = 9) | 7.9 ± 1.8    | 121 ± 26       | 10 ± 1.3     |
| 4-AP               | 3.9 ± 1.4    | 89 ± 12        | 3.4 ± 0.6   |         | 7.2 ± 2.1    | 80 ± 13        | 13 ± 0.8     |
| 4-AP + Nimodipine  | 6.8 ± 0.5*   | 71 ± 5*        | 8.1 ± 0.7*  |         | 3.1 ± 1.1*   | 51 ± 7*        | 19 ± 1.7*    |

4-AP 4-aminopyridine,

\*  $p < 0.05$ ;\*\*  $p < 0.01$ ; n = number of cells.



Table 3

Comparison of previous reports on Ca<sup>2+</sup> currents/channels in SGNs

| Reference               | Preparation                  | Current/s             | Sensitivity  | $\alpha$ -subunit   | Methods             | Predicted functions   |
|-------------------------|------------------------------|-----------------------|--|---|---------------------|---|
| Lv et al., (this paper) | Post-hearing murine SGNs     | L-, N-, P/Q-, RT-type | Cd <sup>2+</sup> , DHPs, $\omega$ -Conotoxin MVIIA, $\omega$ -Agatoxin IVA, rSNX-482, mibefradil | Ca <sub>v</sub> 1.3, Ca <sub>v</sub> 2.1-3, Ca <sub>v</sub> 3.1-3 | EP, IC, WCVC, SC/IM | Spike latency, amplitude, width, AHP<br>Spike frequency and pattern<br>Activation of outward currents |
| (Chen et al., 2011)     | Pre-hearing murine SGNs      | N/A                   | Cd <sup>2+</sup>   | Ca <sub>v</sub> 1.3, Ca <sub>v</sub> 2.2, Ca <sub>v</sub> 3.3     | EP, IC/IM           |   |
| (Lopez et al., 2003)    | Post-hearing chinchilla SGNs | N/A                   | N/A  | Ca <sub>v</sub> 1.2-3, Ca <sub>v</sub> 2.2-3                      | IM                  | Spike shape of APs  |
| (Jimenez et al., 1997)  | Embryonic day E6-17 chicks   | L-, N-type            | Cd <sup>2+</sup> , DHPs, $\omega$ -Conotoxin GVIA  | N/A   | EP, WCVC            | Neuronal development  |
| (Hisashi et al., 1995)  | Post-hearing guinea pig SGNs | L-type                | La <sup>3+</sup> , Cd <sup>2+</sup> , Ni <sup>2+</sup> , Co <sup>2+</sup> , DHPs                 | N/A   | EP, WCVC            | Spike shape of APs  |

DHPs = dihydropyridines, EP = electrophysiology, IC = current clamp, WCVC = whole-cell voltage clamp, SC = single channel recordings, IM = immunolocalization, AP = action potential, AHP = afterhyperpolarization